FOI-R--0364--SE
May 2002
ISSN 1650-1942
User report

The N_4 project. Annual report for the year 2001

Henric Östmark, Martina Bittererová, Tore Brinck, Nathan Hore, Rob Claridge, Rolf Tryman, Sara Wallin, Anna Pettersson, Olli Launila

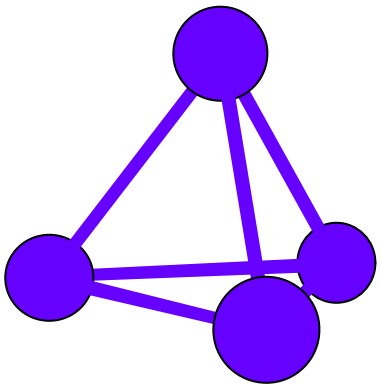

Weapons and Protection
SE-147 25 Tumba

SWEDISH DEFENCE RESEARCH AGENCY
Weapons and Protection
SE-147 25 Tumba

FOI-R--0364--SE
May 2002
ISSN 1650-1942
User report

The N_4 project. Annual report for the year 2001

Henric Östmark, Martina Bittererová[1], Tore Brinck[1], Nathan Hore, Rob Claridge[2], Rolf Tryman, Sara Wallin, Anna Pettersson, Olli Launila

1) Physical Chemistry, Royal Institute of Technology

100 44 Stockholm, Sweden

2) QinetiQ, MoD Fort Halstead, Building R47

Sevenoaks, Kent TN14 7BP, United Kingdom

Issuing organization	Report number, ISRN	Report type
FOI – Swedish Defence Research Agency Weapons and Protection SE-147 25 Tumba	FOI-R--0364--SE	User report
	Research area code 5. Combat	
	Month year May 2002	**Project no.** E2968, E2004
	Customers code 5. Commissioned Research	
	Sub area code 59 Interdisciplinary Projects regarding Combat	

Author/s (editor/s)		Project manager
Henric Östmark	Martina Bittererová	Henriv Östmark
Tore Brinck	Nathan Hore	**Approved by**
Rob Claridge	Rolf Tryman	
Sara Wallin	Anna Pettersson	**Sponsoring agency**
Olli Launila		**Scientifically and technically responsible** Olli Launila

Report title

The N_4 project. Annual report for the year 2001

Abstract (not more than 200 words)

A summary of activities and achievments within the N_4 project during 2001 is presented.

Keywords

DARPA, N_4, HEDM, Energetic Materials, Solid Nitrogen, Cryogenic Matrices

Further bibliographic information	Language English

ISSN 1650-1942	Pages 69 p.
	Price acc. to pricelist

Utgivare
Totalförsvarets Forskningsinstitut - FOI
Vapen och skydd
147 25 Tumba

Rapportnummer, ISRN
FOI-R--0364--SE

Klassificering
Användarrapport

Forskningsområde
5. Bekämpning

Månad, år
Maj 2002

Projektnummer
E2968, E2004

Verksamhetsgren
5. Uppdragsfinansierad verksamhet

Delområde
59 Breda projekt inom bekämpning

Författare/redaktör
Henric Östmark
Tore Brinck
Rob Claridge
Sara Wallin
Olli Launila
Martina Bittererová
Nathan Hore
Rolf Tryman
Anna Pettersson

Projektledare
Henric Östmark

Godkänd av

Uppdragsgivare/kundbeteckning

Tekniskt och/eller vetenskapligt ansvarig
Olli Launila

Rapportens titel (i översättning)
N_4 projektet. Årsrapport för år 2001

Sammanfattning (högst 200 ord)
En sammanfattning över aktiviteter och resultat inom N_4 projektet under år 2001 presenteras.

Nyckelord
DARPA, N_4, HEDM, Energetiska material, Fast kväve, Kryogeniska matriser

Övriga bibliografiska uppgifter

Språk Engelska

ISSN 1650-1942

Antal sidor: 69 s.

Distribution enligt missiv

Pris: Enligt prislista

Contents

Introduction

During 2001, the main efforts within the N_4 project have been concentrated to electric discharge excitation, ion-bombarding and microwave excitation and α-particle excitation experiments on cryogenic nitrogen-containing matrices in two different cryostats. Several synthesis attempts have been made using long integration times in order to suppress random noise. Temperature-controlled experiments have been performed on products from microwave discharge, condensed on a sapphire window in a small cryostat. A time-of-flight mass spectrometer has been used for laser decomposition experiments on high-nitrogen compounds, previously synthesized and characterized through Raman spectroscopy. Initial capillary experiments of liquid nitrogen with multiphoton excitation have been performed at 222.7 nm. SERS (Surface-Enhanced Raman Spectroscopy) experiments have been carried out on previously known substances, including $P_4(T_d)$. A vacuum ultraviolet system has been set up for matrix emission studies in the 120-200 nm range. Extensive theoretical calculations have been performed in order to locate new synthesis and detection pathways for $N_4(T_d)$ and $N_4(D_{2h})$.

Synthesis experiments in cryogenic matrices

After the initial experiments with ion gun (VG Microtech AG5000 ION/8) for the production of N_2^+, N^+ or positive rare gas ions for direct bombardment of cryogenic nitrogen-containing matrices, two additional means of matrix excitation have been tested. A microwave cavity of commercial design (SAIREM GMP 03 KE/D) and a laboratory-built small hollow cathode device. All three devices are mounted simultaneously to the same cryochamber and can be used in parallel. Fig. 1 shows a picture of the cryostat with the microwave discharge running on pure neon.

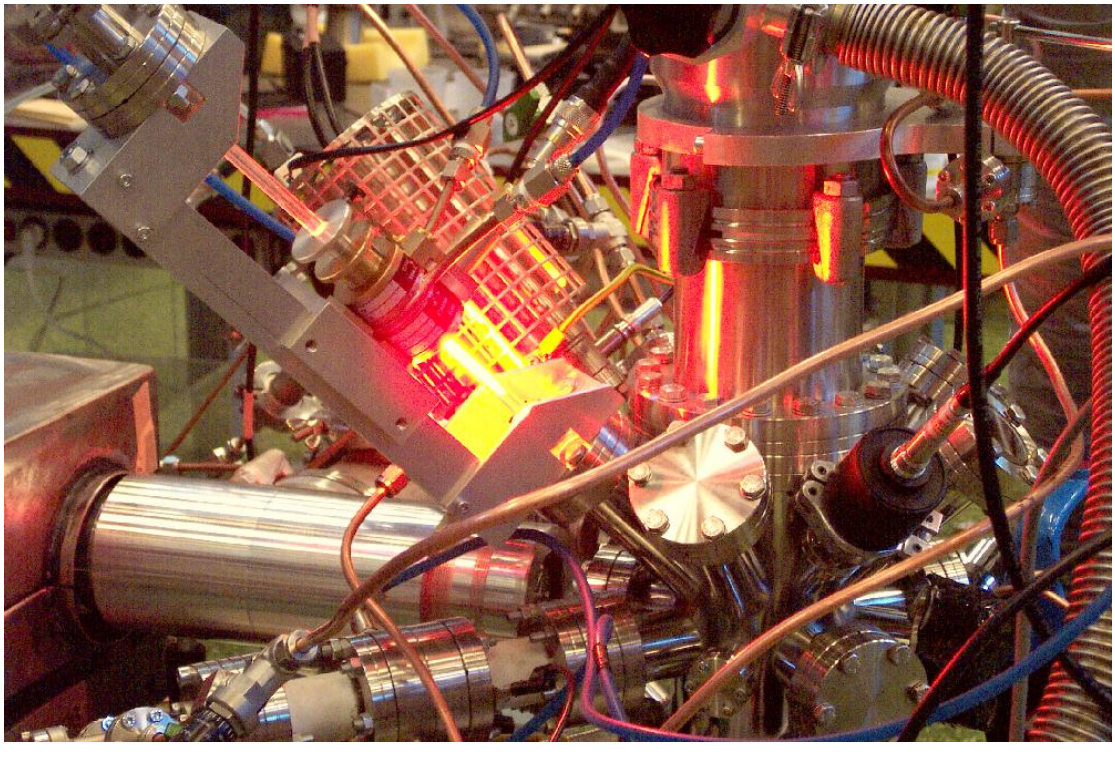

Fig. 1. Three matrix excitation devices, mounted on the same cryostat. The miniature hollow cathode is seen in the lower left. In the middle, the microwave cavity is seen running on pure neon. The protection shield of the ion gun is seen behind the discharge. The aluminum tube below the ion gun contains the lens system (cf. Fig. 2).

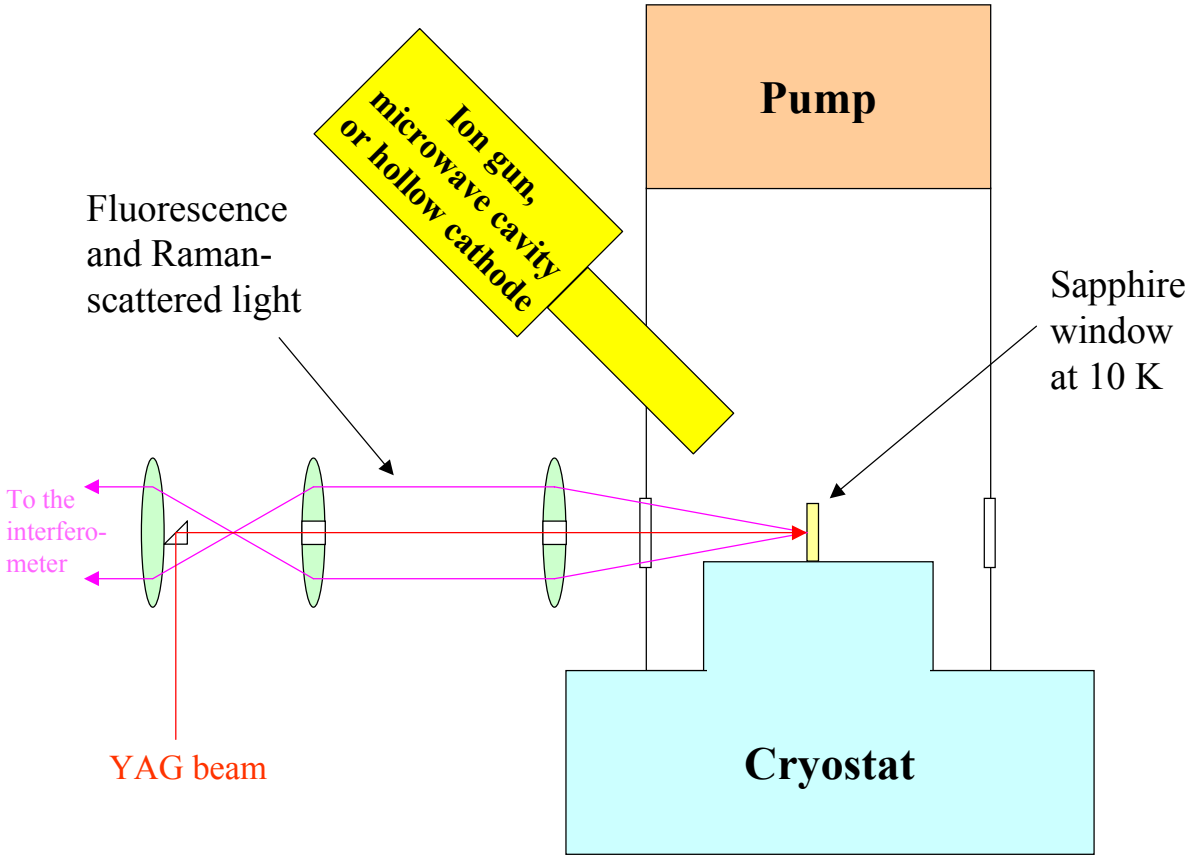

Fig. 2. Schematic arrangement of the matrix excitation experiments. A cryogenic matrix, consisting of pure nitrogen or a mixture of nitrogen with different nitrogen-containing species is first deposited on the sapphire window. During the deposition, the Raman signal is continuously monitored with a FT-Raman interferometer. When a desired matrix thickness has been reached, the matrix is bombarded with ions (N_2^+, N^+, Ar^+, Ne^+ or He^+) or corresponding products from a microwave or a hollow cathode discharge. The resulting matrix fluorescence is monitored with an IFS55/FRA106 FT-Raman interferometer and a Mechelle 900 UV-VIS-NIR spectrometer.

When the cryostat cold finger is cooled and when the discharge contains enough nitrogen, the deposited nitrogen glows in bright green (Fig. 3)

Fig. 3. The cryostat sapphire window, photographed under nitrogen deposition from microwave discharge. The sapphire window is located in the circular aperture of the rectangular copper block, mounted on the cold finger. The transparent, very thin nitrogen matrix is photographed from behind. The magenta-colored orifice of the microwave capillary is seen to the upper left. The green color arises from a ^2D-^4S transition in nitrogen atoms in the deposited solid, while the magenta color of the capillary tube is due to the $C^3\Pi_u$-$B^3\Pi_g$ and $B^3\Pi_g$-$A^3\Sigma_u^+$ emissions in N_2.

Numerous synthesis experiments have been carried out on excited, nitrogen-containing matrices during 2001. All three excitation devices mounted on the cryostat have been used in these experiments. Four different types of recordings have been made:

1. *Recordings of a matrix during the excitation phase (relatively short recordings during several hours of matrix build-up).*
2. *Long-time recordings of the matrix after excitation (FT-Raman)*
3. *Short time series during rapid warm-up of the excited matrix.*
4. *Extended time series during gradual stepwise warm-up of the excited matrix.*

Different types of information can be collected in these experiments. During the excitation phase, mixed spectra of gas-phase and matrix processes are obtained with the FT-Raman instrument either in Raman mode (laser on) or in infrared emission mode (laser nearly off). Simultaneous spectra are recorded with the Mechelle 900 UV-VIS-NIR spectrometer. Together, these instruments cover the wavelength range of 200-1800 nm. The gas phase spectra most often consist of well-known molecular N_2 or N_2^+ bands, together with rare gas atomic emission spectra in the cases where mixtures of rare gases and N_2 have been used. In the case of microwave discharges, the $B^3\Pi_g$-$A^3\Sigma_u^+$ system of N_2 usually dominates, while the hollow cathode device also gives N_2^+, as well as higher-lying excited states of N_2.

In the long-time recordings (exceeding 14 hours), mostly the FT-Raman instrument has been used. These recordings give highly puzzling spectra, where the most dominating features are still unassigned. One of the unassigned features is a characteristic triplet, consisting of two close-lying strong lines and a weaker one, shown in Fig. 4.

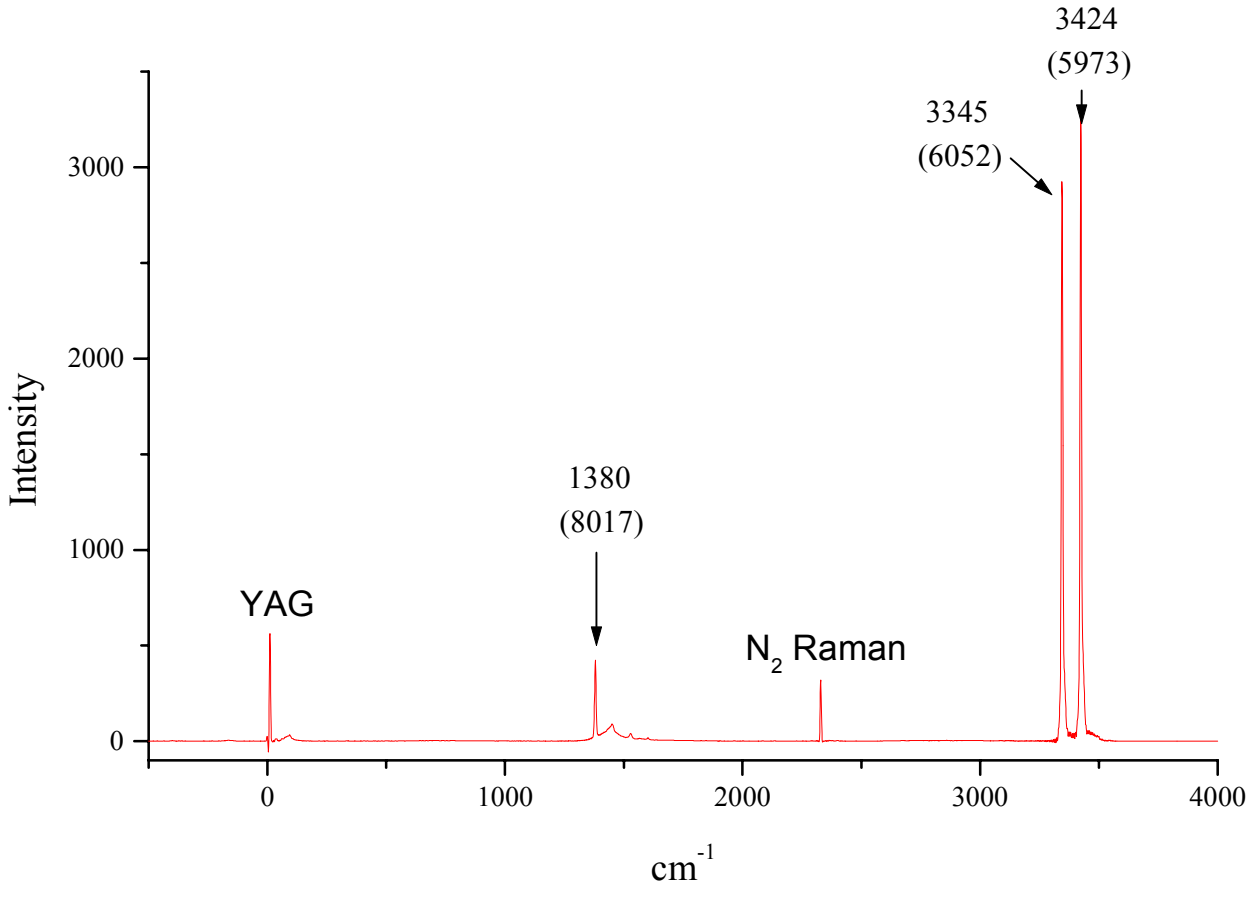

Fig. 4. A long-time FT-Raman recording (28000 scans in 14 hours) of a microwave discharge-excited N_2 matrix. The apparent wavenumbers of the triplet are shown, as given by the interferometer software, together with the true fluorescence wavenumbers in parenthesis. The YAG power was 500 mW and the resolution 4 cm^{-1}.

This triplet is laser-induced, and its intensity is linearly dependent on the YAG power. Clearly, the triplet is not due to a Raman process, as has been shown in isotopic substitution experiments (Fig. 5).

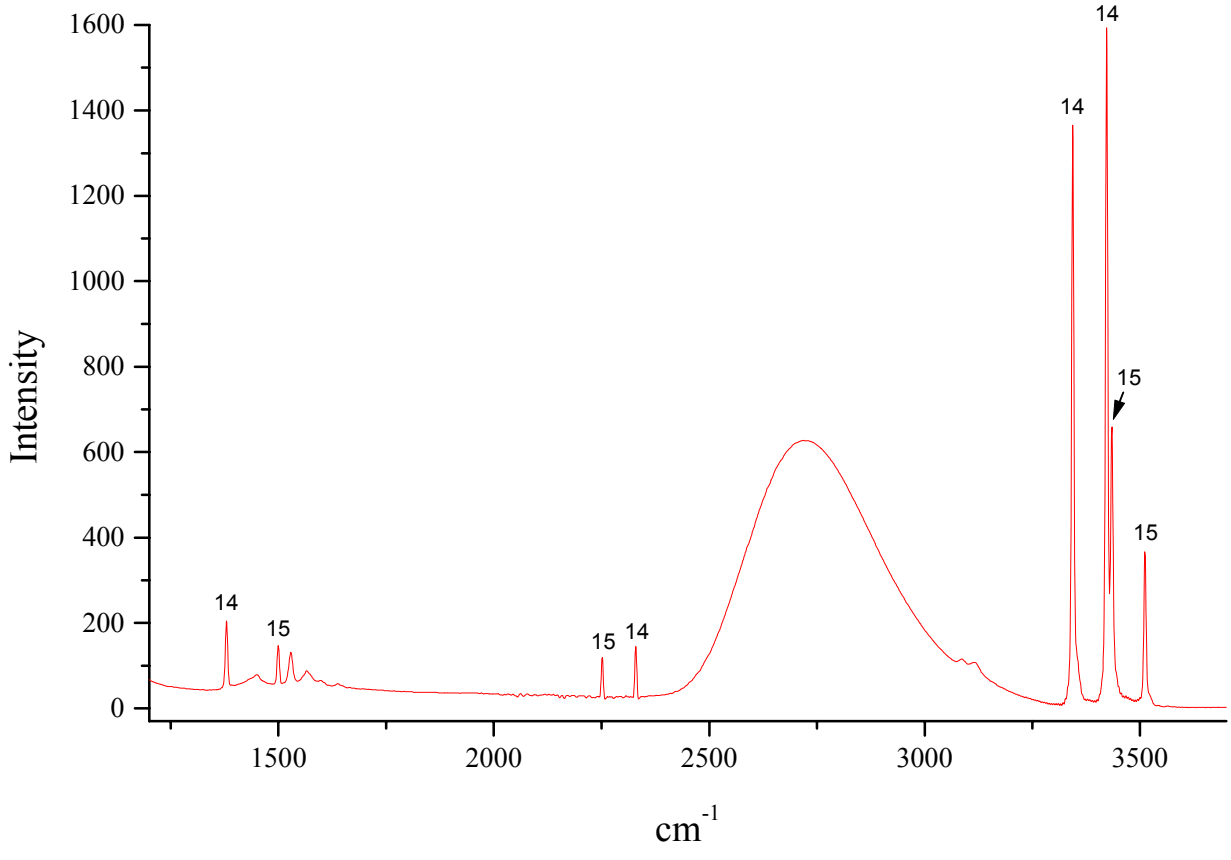

Fig. 5. Long-time FT-Raman recording (33000 scans in 16½ hours) of a $^{14}N_2$+$^{15}N_2$ matrix, excited by ion gun, running on pure $^{14}N_2$, pure $^{15}N_2$ and on a mixture of these. The two lines in the 2300 cm^{-1} region are the N_2 Raman lines for both isotopomers. No sign of $^{14}N^{15}N$ was seen. The fact that the triplet lines move to higher (apparent) wavenumbers, means that they cannot be Raman lines. The YAG power was 500 mW and the resolution 4 cm^{-1}.

The triplet has been investigated more closely in an isotopic replacement experiment. The ion gun was first run with pure $^{14}N_2$ in order to establish proper conditions for the triplet build-up. When these conditions were found, pure $^{15}N_2$ was introduced in the ion gun. We observed that the N_2 Raman line moved as it should (towards lower Raman wavenumbers), while the triplet lines moved to the opposite direction (Fig. 5).

This behavior is consistent with the assumed fluorescence origin of the triplet. In the following table, the true wavenumbers are used for these lines.

σ_{14}	σ_{15}	σ_{14}/σ_{15}	**Commentary**
2329.29	2251.59	1.0345	N_2 Raman
8016.95	7897.07	1.0152	LIF (weak)
6052.33	5961.25	1.0153	LIF (strong)
5973.26	5884.51	1.0151	LIF (strong)

What could be considered as intriguing, is that only two different triplet spectra are observed, despite the fact that the matrix contains $^{14}N_2$ and $^{15}N_2$ in approximately equal concentrations, as can be seen by looking at the intensities of the N_2 Raman lines. According to our opinion, this clearly excludes N_4 as a carrier (rectangular or tetrahedral), since such a molecule should occur in at least three different isotopic configurations in the matrix ($^{14}N_2$+$^{14}N_2$, $^{14}N_2$+$^{15}N_2$ and $^{15}N_2$+$^{15}N_2$), which should result in three distinct spectra. On the other hand, the carrier must contain nitrogen in a rather tightly bound position, because the isotopic shift is quite substantial.

The unassigned triplet occurs in all three investigated types of excitation, being strongest in hollow cathode- and microwave-excited matrices. In Ref. [5], the relative intensities within the triplet were given as 5, 44 and 51 percent of the total intensity carried by the triplet. In these values, the influence of the detector response curve had not been taken into account. The above measurements with a white light source show now that the correct numbers are actually 5, 28 and 67 per cent, respectively. In Ref. [5], a comparison was also made between the intensity carried by the N_2 Raman line and the total intensity of the triplet. If the obtained result (3 per cent) is corrected with respect to the detector curve, we now obtain only 1 per cent for the contribution of the N_2 Raman line as compared to the triplet. This result is even more remarkable than the previous one, and certainly warrants a thorough examination.

The third type of experiment consists of heating the matrix from 10 K to 30 K by gradually applying an increasing current to a resistor, in thermal contact with the matrix. These experiments often give characteristic structured emissions in the infrared and in the visible. The matrix emission mostly consists of atomic N spectra (^2P-^2D and ^2D-^4S), bearing witness of atom-matrix interactions through the occurrence of characteristic vibron- and phonon-induced sidebands. The processes can largely be explained by recombination schemes, where free nitrogen atoms are involved. A pair of ^4S nitrogen atoms lies at an energy of 9.8 eV, compared with a N_2 molecule in the ground state. A process like $N(^4S) + N(^4S) \rightarrow N_2(A^3\Sigma_u^+)$ is exothermal by several eV. The 6.2 eV energy stored in $N_2(A^3\Sigma_u^+)$ is subsequently used to pump up N atoms to the ^2D or ^2P states at 2.4 and 3.6 eV, respectively, causing the intensive green ($^2D \rightarrow ^4S$) and IR ($^2P \rightarrow ^2D$) emissions, which persist as long as fresh $N(^4S)$ supply is guaranteed. Another aspect of this process, dealing with α-particle excitation of N_2, has been described in Ref. [10]. Many features in the warm-up spectra coincide with the spectra recorded under excitation, although the relative intensities differ considerably.

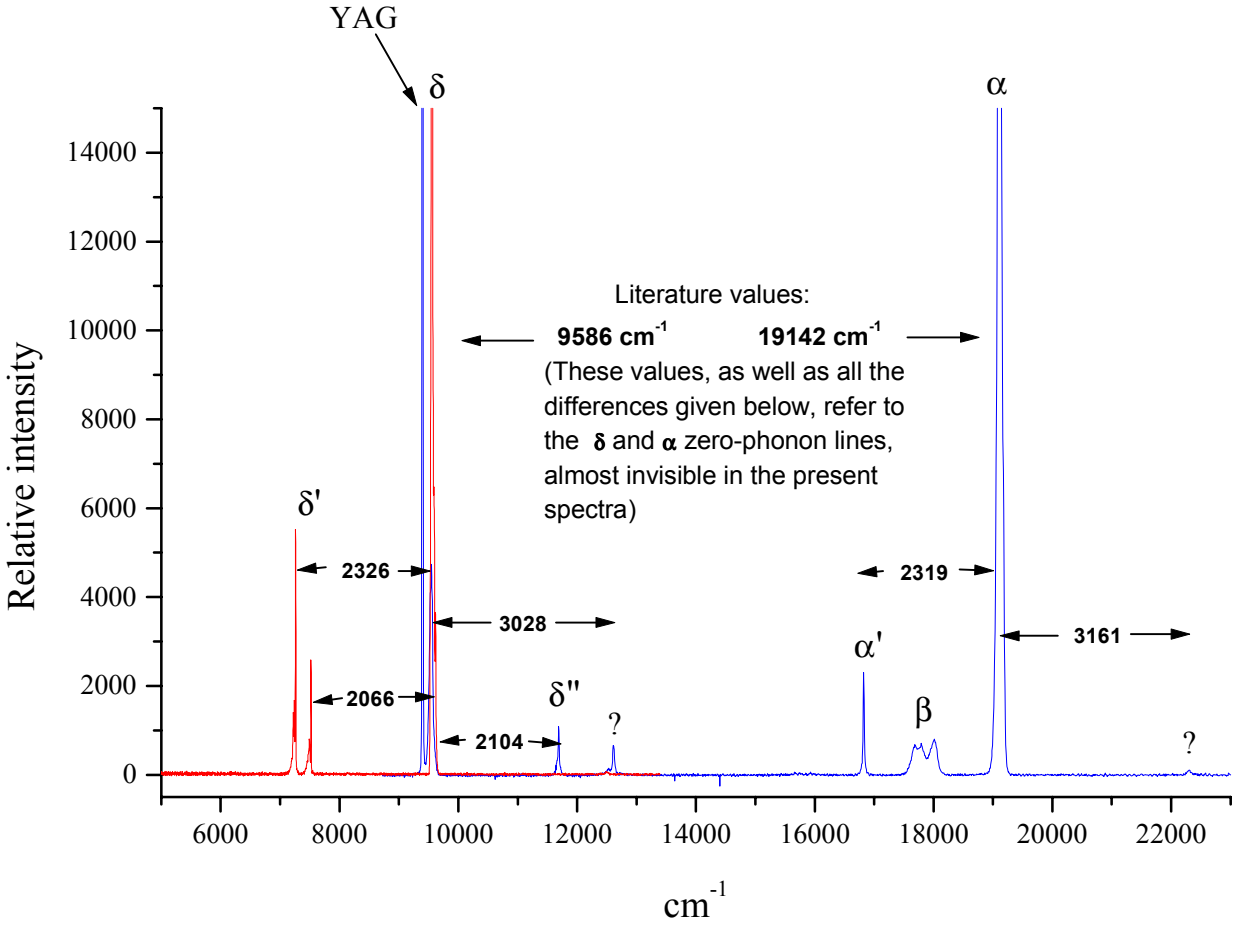

Fig. 6. Combined FT- and Mechelle-spectra during the warm-up of a nitrogen matrix. The α and δ lines correspond to the atomic nitrogen ^2D-^4S and ^2P-^2D transitions, respectively. The α' and δ' lines are corresponding vibrational satellites. Several weaker lines near the δ line have not been assigned. The β line has been assigned as a ^1S-^1D transition in atomic oxygen. The oxygen atoms are presumably released from the quartz capillary through the influence of the discharge. The YAG power was very low (8 mW). The integration time was 30 s.

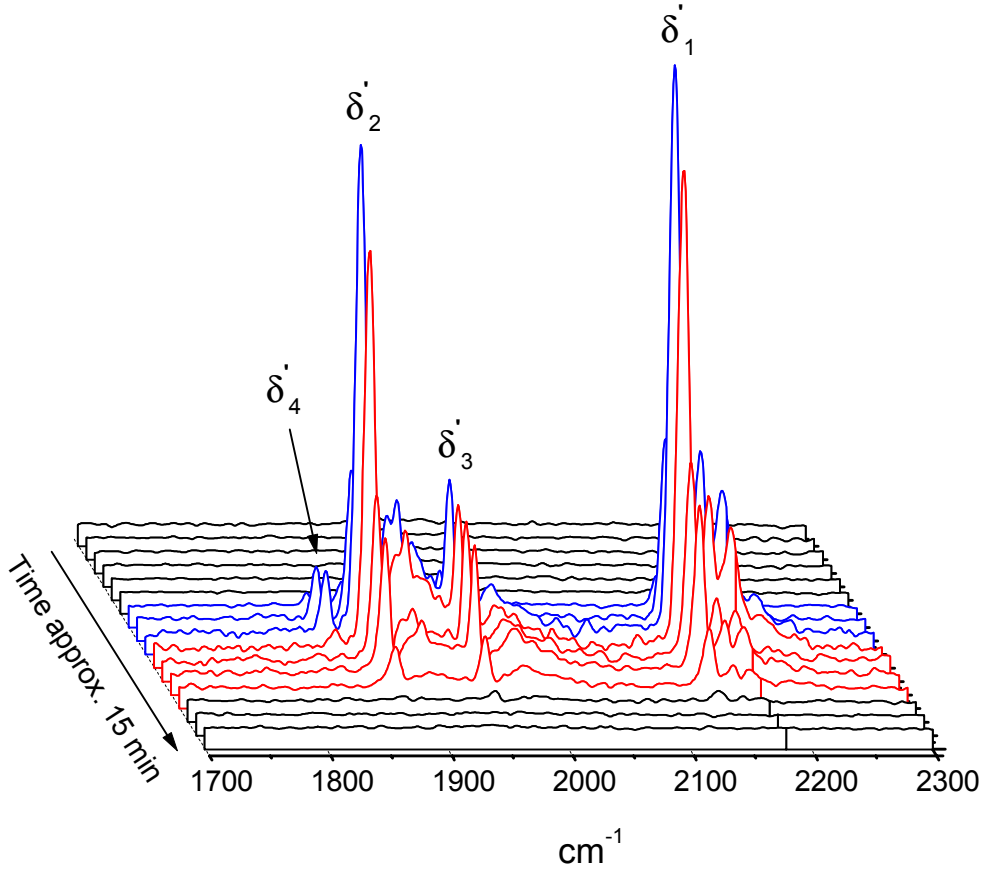

Fig. 7. A warm-up spectrum of the δ' group in a nitrogen matrix. The matrix was built up during 2½ hours using a hollow cathode discharge in pure N_2. The δ_1' band is attributed to the ^2P-^2D transition in nitrogen atom, combined with a simultaneous vibrational excitation of a neighboring N_2 molecule. The remaining bands are unassigned so far. An isotopic substitution experiment on the δ' group is shown in Fig. 8.

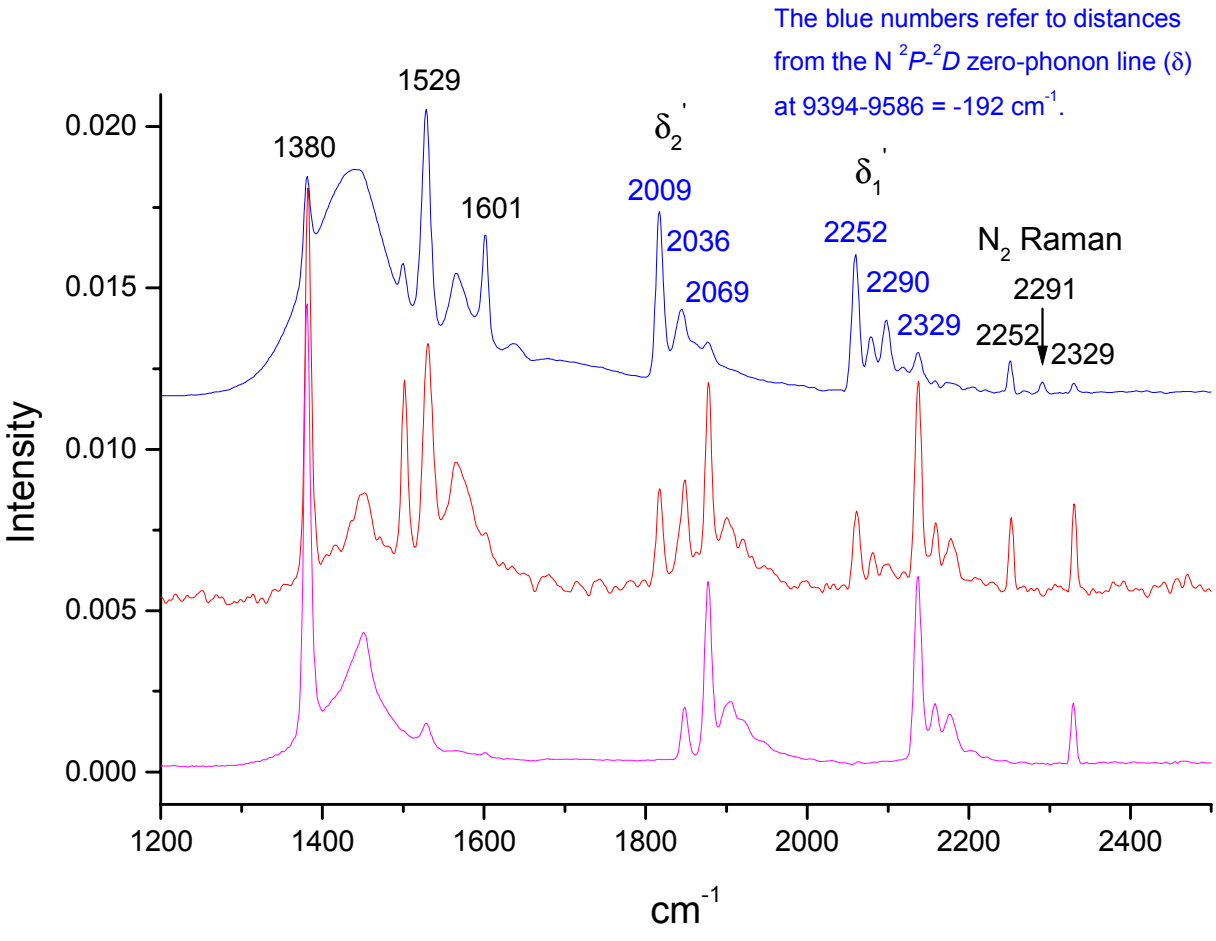

Fig. 8. Isotopic substitution experiment on the δ' group in a nitrogen matrix. The present spectra were recorded during the warm-up phase of two matrices, built up using a microwave discharge in pure $^{14}N_2$ (magenta) and in mixtures of $^{14}N_2$ and $^{15}N_2$ (red and blue). In the blue spectrum, we now have a substantial concentration of $^{14}N^{15}N$ in the matrix, as seen by its Raman line at 2291 cm^{-1}. Observe that the blue numbers in the spectra are measured from a different origin (-192 cm^{-1}). The Raman lines at 2252, 2291 and 2329 are due to the $^{15}N_2$, $^{14}N^{15}N$ and $^{14}N_2$ species, respectively. The intensity enhancements in the δ'$_1$ subgroup at 2290 and 2329 cm^{-1} (in blue) are consistent with the $^{14}N^{15}N$ and $^{15}N_2$ Raman intensities, while the δ'$_2$ subgroup is difficult to interpret. The features at 1529 and 1601 cm^{-1} are due to the YAG-excited $a^1\Delta_g \rightarrow X^3\Sigma_g^-$ bands of O_2, often present as impurity due to quartz tubing of the discharge.

Yet another type of experiment consists of switching off the excitation source and recording time series (Fig. 9). Long integration times can be used since some of the de-excitation processes are very slow (30-100 s). An average of two of the spectra of the time series of Fig. 9 is shown in Fig. 10. The unassigned features in these spectra are probably due to different species.

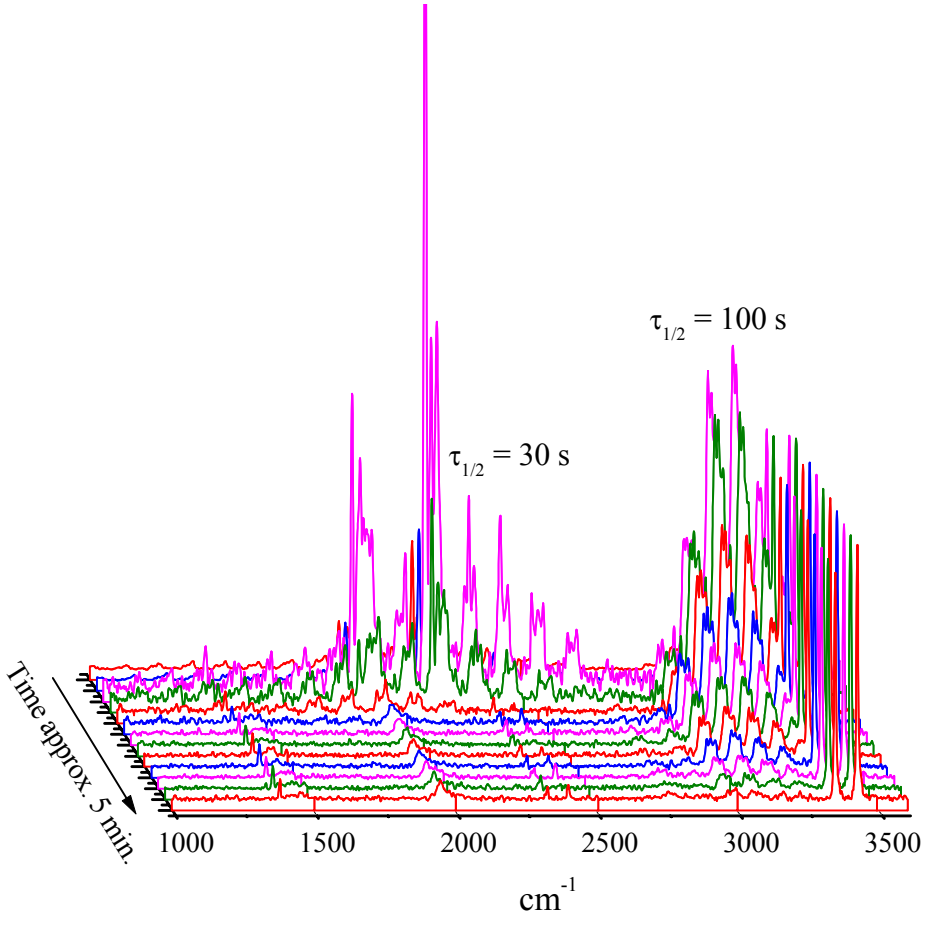

Fig. 9. A time series of excited N_2 matrix at 10 K, recorded after sudden switching-off of the hollow cathode excitation discharge. The spectra represent consecutive 20-scan FT-Raman recordings with a YAG power of 500 mW and resolution 4 cm^{-1}. Two characteristic decay times are observed for the two different (unassigned) band systems in the 2000 cm^{-1} and 3200 cm^{-1} regions, respectively. The conclusion is that there are two different carriers involved.

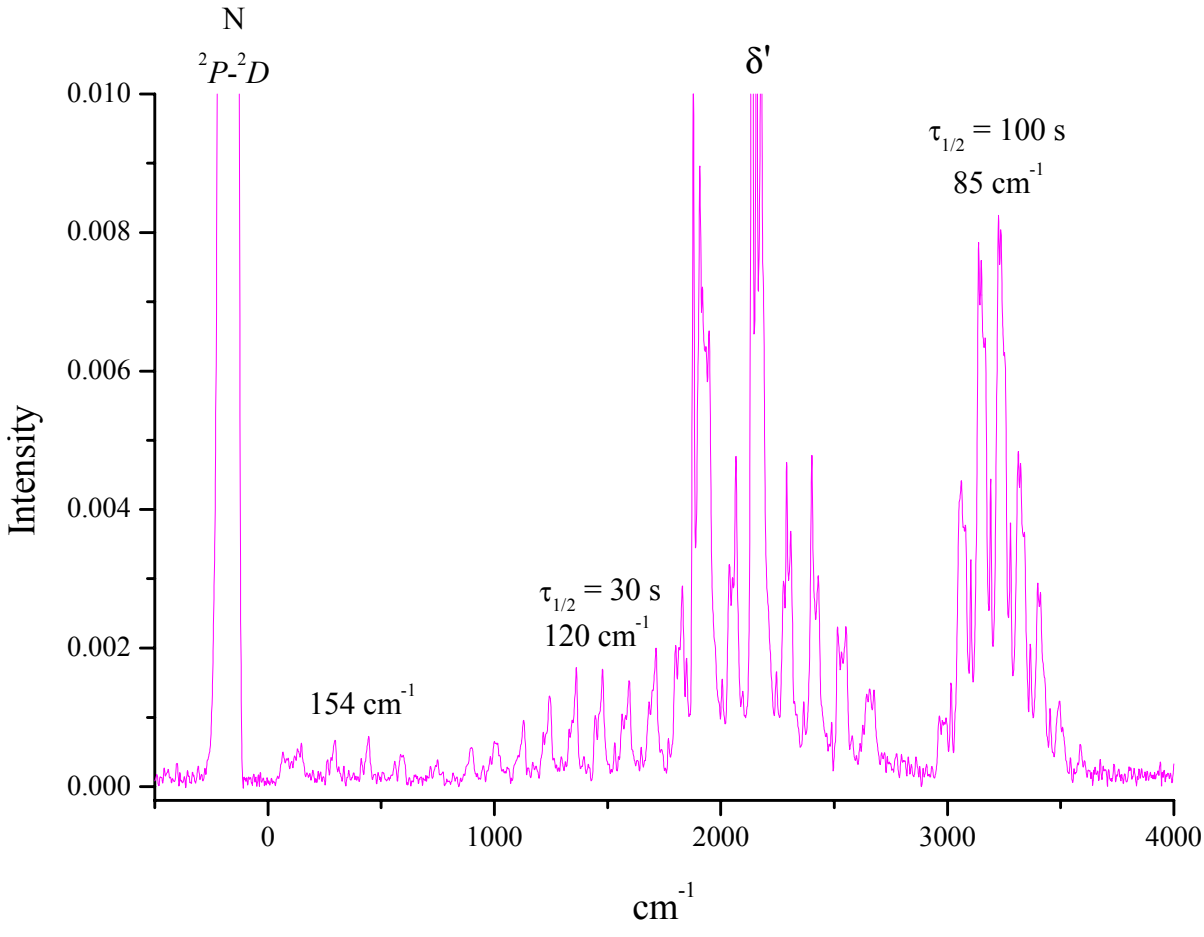

Fig. 10. An average of two of the spectra in the time series of Fig. 9. The wavenumber designations in the spectra refer to the characteristic sub-band separations within the corresponding band systems. In the case of the 3200 cm^{-1} band system, the sub-bands can be fitted to a first-degree polynomial, while a second-degree polynomial is needed for the 2000 cm^{-1} system.

Upon annealing, the triplet vanishes completely (and irreversibly) at 37 K, as can be seen in Fig. 11. Interestingly, this is approximately the temperature of the α→β phase transition in solid nitrogen (35.6 K).

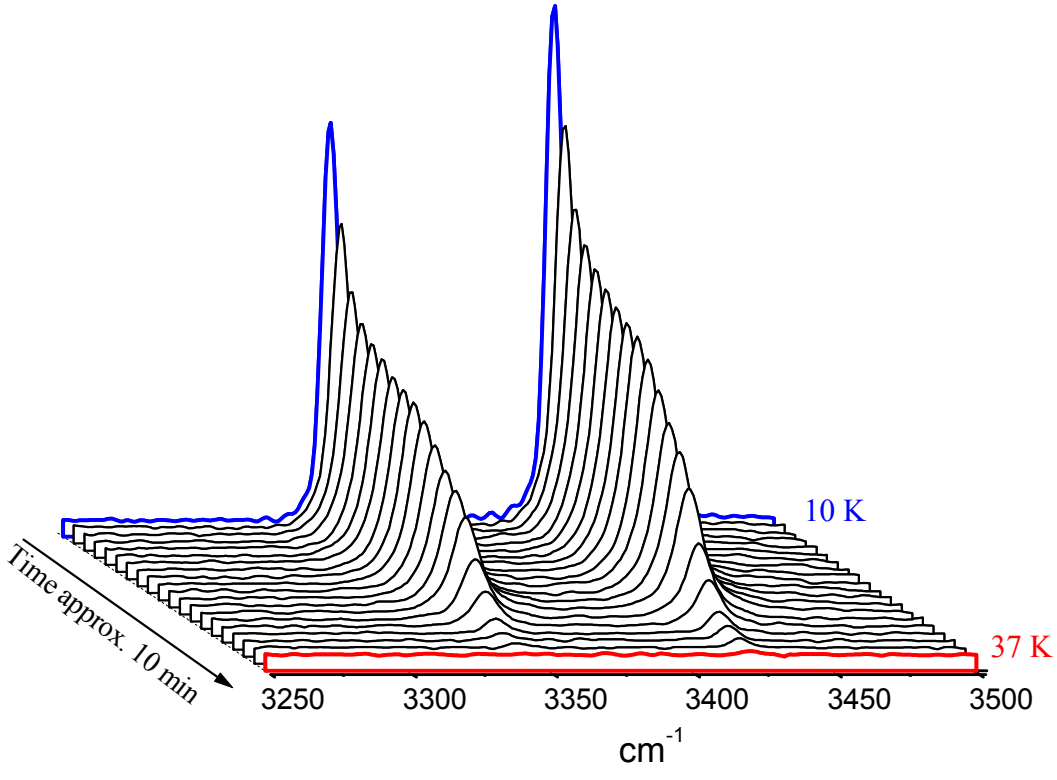

Fig. 11. The 3400 cm^{-1} doublet, recorded during 10 minutes after compressor shut-off. Each individual spectrum represents an average of 20 scans. The laser power was 500 mW and resolution 4 cm^{-1}.

We have now collected a rather large material on processes in excited cryogenic matrices. A critical evaluation of this material boils down to some important conclusions, regarding the possibility of a successful synthesis and detection of $N_4(T_d)$ in cryogenic matrices. First of all, some of the unassigned features shown above may constitute important precursors in the synthesis efforts. In particular, the origin of the mysterious triplet has to be established with certainty. Another important feature in the spectra is the unexpectedly complicated δ' group. The unexplained lines in this group might in fact arise from a hitherto unknown carrier (possibly an isomer of N_3). The even more complicated features shown in Figs. 9-10 represent a veritable challenge, since they are difficult to reproduce and decay rapidly once the discharge is turned off.

Perhaps the most important conclusion is that we have been able to deposit, excite and manipulate our matrices in a largely reproducible manner. This means that a foundation has now been laid for cryosynthesis experiments, where free nitrogen atoms are to be used as reactants in the continuing efforts to synthesize $N_4(T_d)$. A very important idea has arisen during the present experiments. This idea consists of trying to use triangular N_3 for this synthesis according to the scheme: $N_3(C_{2v}) + N(^2D) \rightarrow N_4(T_d)$.

A new synthesis route for $N_4(T_d)$

We have performed calculations on the hitherto not reported triangular $N_3(C_{2v})$ radical. Detailed calculations on this species clearly show that the radical is bound. This means that we now have a new precursor for the $N_4(T_d)$ synthesis according to the scheme: $N_3(C_{2v}) + N(^2D) \rightarrow N_4(T_d)$.

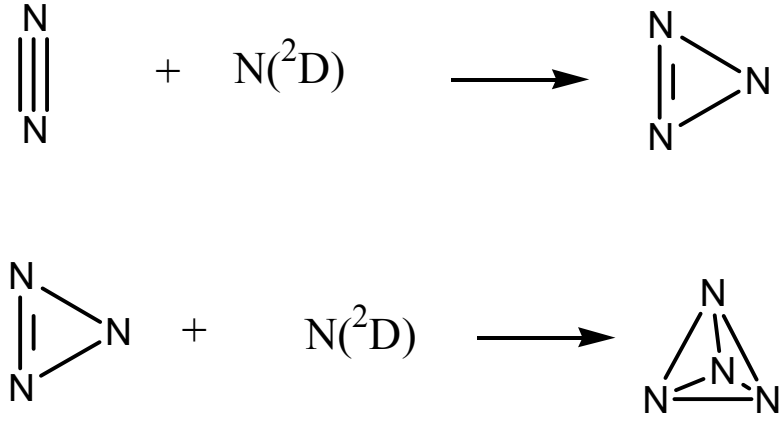

Fig. 12. A new proposed synthesis route for N_4. Both steps are fully symmetry-allowed and exothermal. The scheme works in cryogenic environments, where $N(^2D)$ can be generated from previously deposited ground state nitrogen atoms using the following two-step process: **1.** $N(^4S)+N(^4S) \rightarrow N_2(A^3\Sigma_u^+)$ **2.** $N_2(A^3\Sigma_u^+) + N(^4S) \rightarrow N_2(X^1\Sigma_g^+) + N(^2D)$.

For this scheme to be realistic, sufficient concentrations of nitrogen atoms must be available in the matrix [9]. If the matrix temperature is raised enough in order to allow sufficient diffusion of N atoms to take place (to 12-15 K), there will be enough time for the first reaction to occur easily, since the lifetime of $N(^2D)$ in a nitrogen matrix is very long (approximately 37 s). Thus, a small concentration of $N_3(C_{2v})$ will hopefully build up, along with the (probably unavoidable) linear $N_3(D_{\infty h})$ radical. The relative cross-sections of these two processes are not known at present. However, once the

experimental vibrational frequencies of $N_3(C_{2v})$ have been experimentally measured, an absorption set-up can be used in order to monitor the respective concentrations of $N_3(C_{2v})$ and $N_3(D_{\infty h})$. The second step in the above scheme will be the overall rate-limiting one, since it involves two low-concentration species. However, if it can be experimentally verified that $N_3(C_{2v})$ can be obtained in measurable quantities in the first step, the second step to the detection of $N_4(T_d)$ will not be a long one.

The main processes to be considered are the following:

Step	**Process**	**Energy release (eV)**
1.	$N(^4S) + N(^4S) \rightarrow N_2(A^3\Sigma_u^+)$	3.6
2.	$N(^4S) + N(^4S) \rightarrow N_2(X^1\Sigma_g^+)$	9.8
3.	$N_2(A^3\Sigma_u^+) \rightarrow N_2(X^1\Sigma_g^+) + h\nu$	6.2
4.	$N_2(A^3\Sigma_u^+) + N(^4S) \rightarrow N_2(X^1\Sigma_g^+) + N(^2P)$	2.6
5.	$N_2(A^3\Sigma_u^+) + N(^4S) \rightarrow N_2(X^1\Sigma_g^+) + N(^2D)$	3.8
6.	$N(^2P) \rightarrow N(^2D) + h\nu$	1.2
7.	$N(^2D) \rightarrow N(^4S) + h\nu$	2.4
8.	$N_2(X^1\Sigma_g^+) + N(^2D) \rightarrow N_3(D_{\infty h})$	2.5
9.	$N_2(X^1\Sigma_g^+) + N(^2D) \rightarrow N_3(C_{2v})$	1.4
10.	$N_3(C_{2v}) + N(^2D) \rightarrow N_4(T_d)$	5.6

The overall reaction for the steps 1-7 is essentially: $2n\mathbf{N} \rightarrow n\mathbf{N_2}$ + photons. The number of emitted photons depends on the actual branching ratios for the steps in question. These ratios are not known at present. If only steps 1-7 are involved, all the energy initially stored in the N atoms is ultimately wasted, since it is converted to photons (in addition to some extent of warming of the matrix, due to vibrational relaxation processes). In order to synthesize N_4 in a matrix, it is therefore necessary to control the steps 8-10, especially the branching ratios involved in steps 8 and 9. This control is most conveniently performed using an absorption set-up for on-line monitoring of the $N_3(D_{\infty h})$ and $N_3(C_{2v})$ concentrations. A preliminary calculation on $N_3(C_{2v})$ at the B3LYP-AVDZ level gives the vibrational frequencies 351, 905 and 1729 cm^{-1}, with the corresponding IR intensities of 12.88, 0.24 and 4.19 km/mol, respectively. At the same level, the calculated frequencies of the linear $N_3(D_{\infty h})$ radical were 472, 1372 and 1714 cm^{-1}, with IR intensities 9.06, 0 and 222.41 km/mol, respectively. More detailed calculations are underway in order to determine the absorption spectrum of $N_3(C_{2v})$, as well as the relevant Raman and IR-absorption cross-sections for both N_3 species.

We have performed long-time diffusion experiments on N_2 matrices containing atomic nitrogen, deposited through a hollow cathode discharge. A typical long-time recording is shown in Fig. 13. In this experiment, the temperature of the matrix was kept at 12.5 K, which allowed some diffusion of N atoms to take place, which is manifested through the observed decay of the green N ^2D-^4S signal.

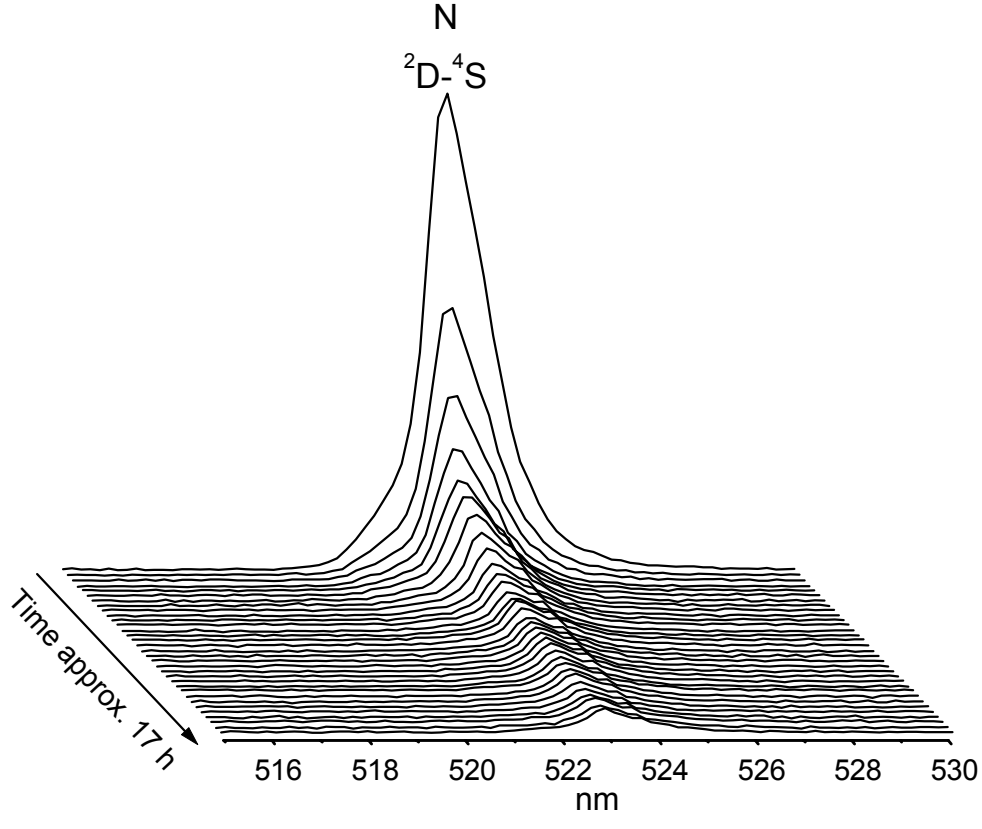

Fig. 13. A long-time recording of a slightly heated (12.5 K) nitrogen matrix, containing free N atoms. The peak shows the time decay of the green ^2D-^4S line of N

The decay of the N ^{2}D-^{4}S green line can be fitted to a double exponential (Fig. 14). The actual meaning of the two characteristic decay times (30 and 165 minutes) is under investigation at present.

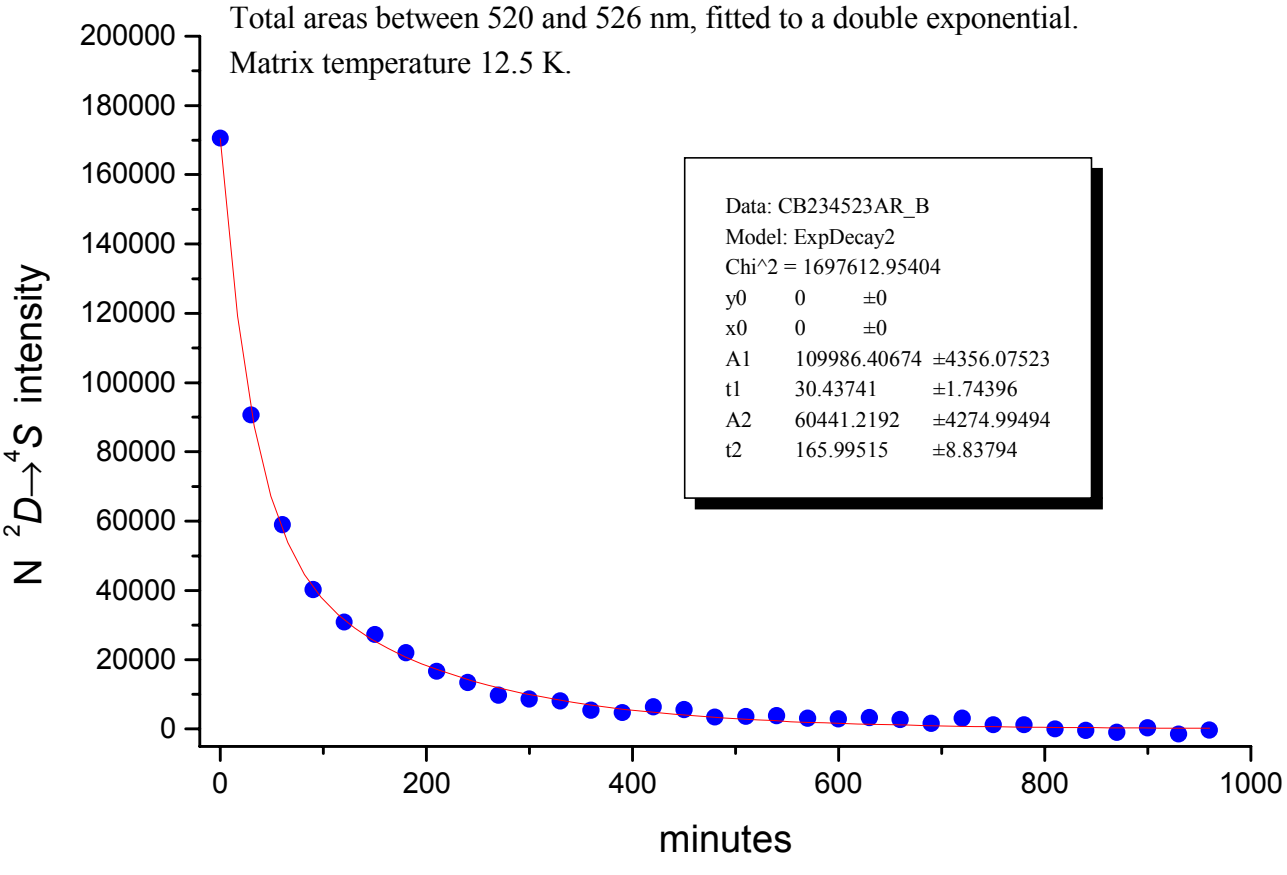

Fig. 14. Total peak areas of the N ^{2}D-^{4}S emission in Fig. 13, fitted to a double exponential. At this temperature (12.5 K), the characteristic decay times are 30 and 165 minutes, respectively.

The potential feasibility of the $N_4(T_d)$ synthesis using the scheme outlined in Fig. 12 is based on the calculations shown in Figs. 15 and 16.

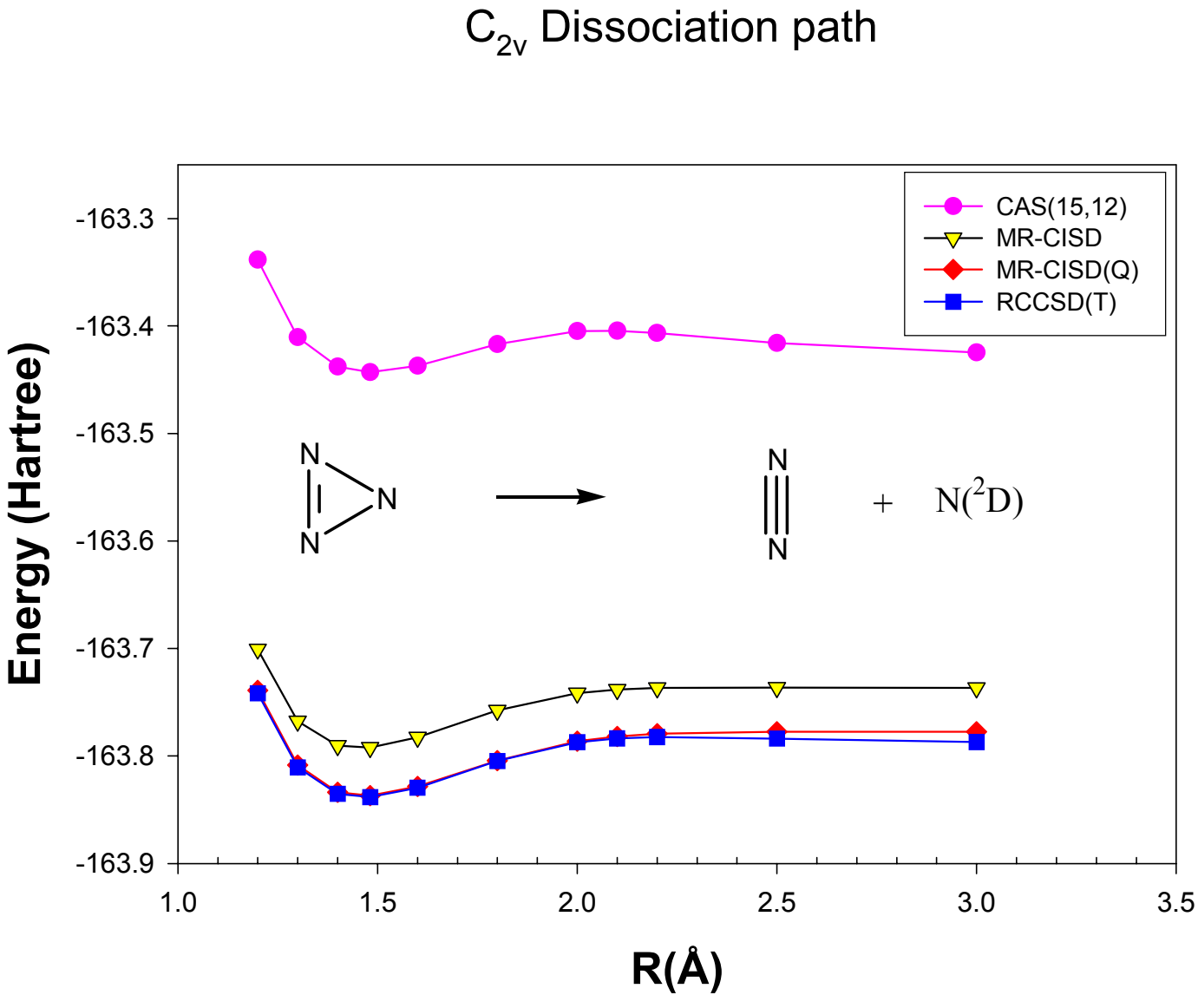

Fig. 15. QM calculations on the dissociation pathway of $N_3(C_{2v})$, performed at various levels. The dissociation energy is approximately 1 eV in all the calculations. This means that $N_3(C_{2v})$ is stable enough to be kept in cryogenic matrices as a precursor for the $N_4(T_d)$ synthesis.

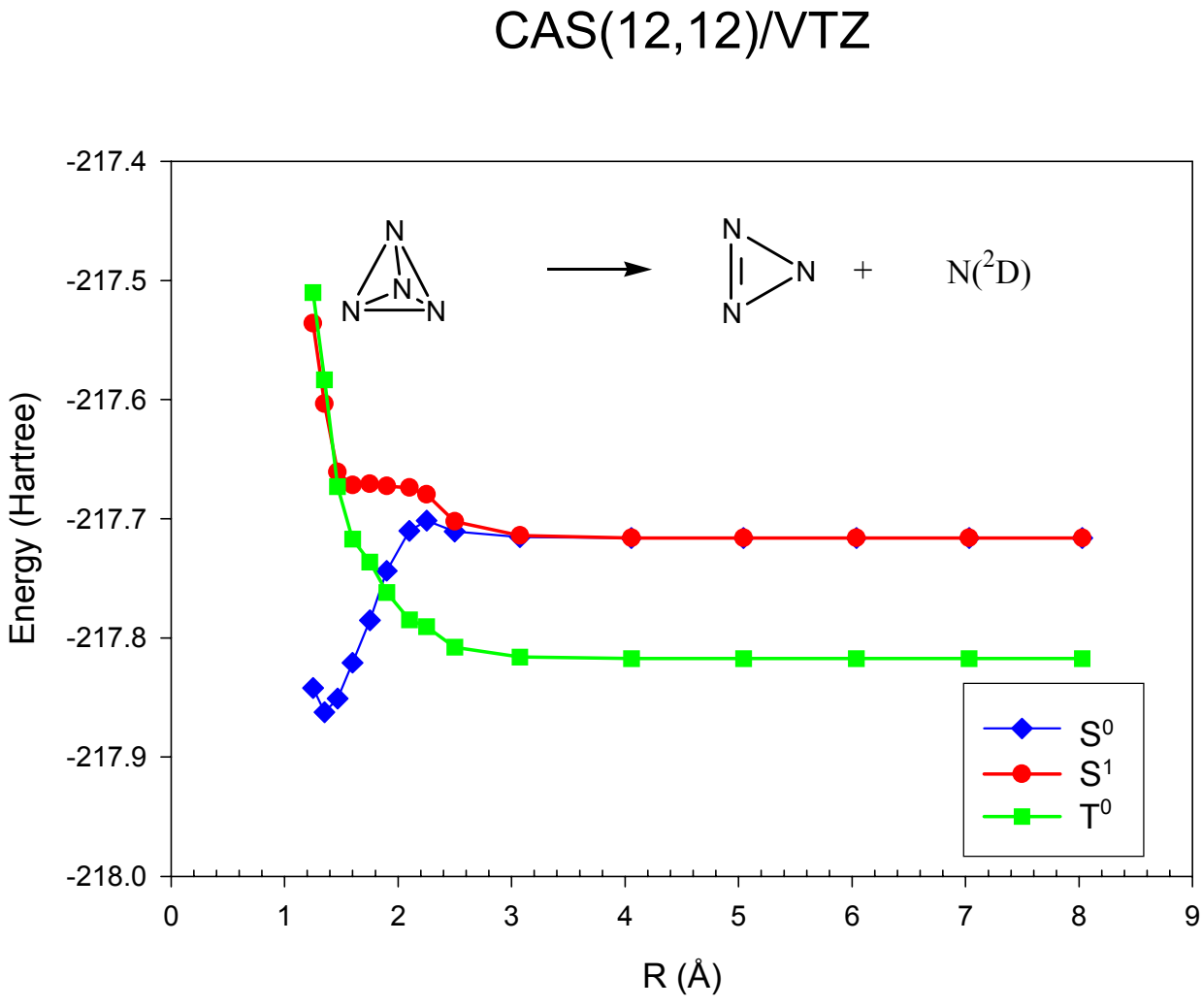

Fig. 16. QM calculations on the dissociation pathway of $N_4(T_d)$, performed at CAS(12,12) level. The dissociation energy of $N_4(T_d)$ in its singlet ground state (blue curve) is approximately 4.7 eV at this level.

Experiments in a temperature-controlled cryostat

A CRYOCOOLER cryostat has been set up for temperature-controlled Raman experiments on matrices, built from microwave discharge products. The basic idea for these experiments is to avoid dilution of possible N_4 products through the excessive condensation of nitrogen, as has been the case for the LEYBOLD cryostat experiments. The laser excitation experiments on solid nitrogen, mentioned in Ref. [10], can also be carried out using this set-up. The experimental equipment is shown in Fig. 17.

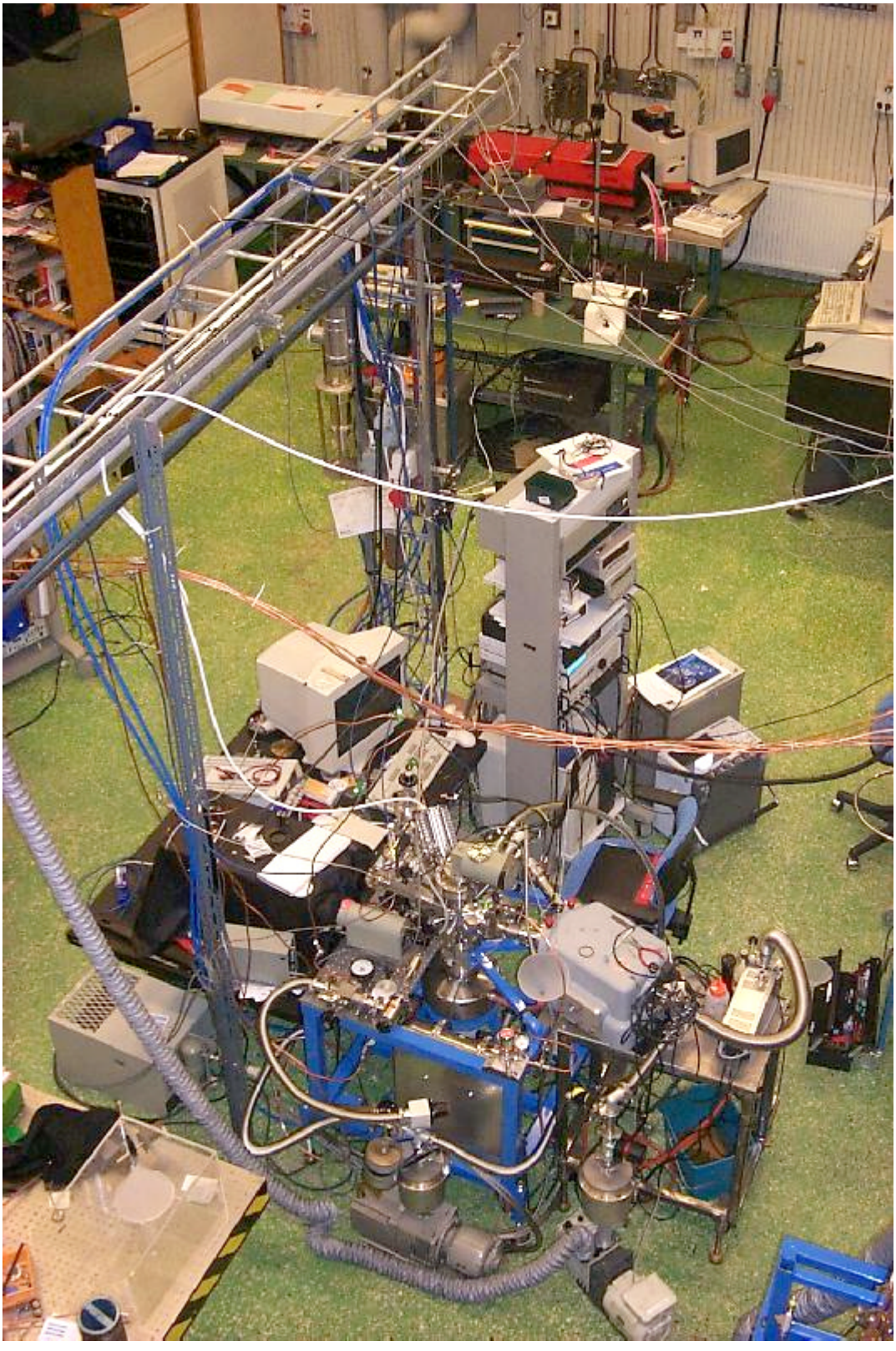

Fig. 17. The experimental set-up for the temperature-controlled experiments on cryogenic matrices. The cryostat, the SPEX 500M and the McPherson 218 VUV monochromator are seen in the lower part. The Ar^+ ion laser (black) is located in the upper part of the figure.

The set-up of the CRYOCOOLER cryostat for Raman measurements with an Ar^+-laser has now been improved by enhancing the laser intensity reaching the matrix. This has been achieved by changing to a more suitable optical fiber and by designing a more efficient coupling of the fiber to the inside of the vacuum chamber. In the new design, a ball lens has also been mounted at the fiber end facing the matrix.

The equipment for the temperature-controlled experiments has now been tested. In these experiments, the microwave discharge has been run on different nitrogen-containing mixtures during extended periods of time, while keeping the sapphire window of the cryostat at a temperature above 77 K, in order to avoid condensation of nitrogen. Experiments done before the Ar^+-laser and spectrometer had been set up for Raman spectroscopy on the matrix showed, that under some conditions an unknown substance was formed on the window when depositing at 77 K. The substance seemed to remain on the window even after the cryostat had returned to room temperature. These experimental conditions have not been tested since the improvement of the Raman setup was made. Long time deposition under similar conditions will be made soon and the deposited substances will be analyzed using Raman spectroscopy with the 514.5 nm line of the Ar^+-laser, in combination with a notch filter (ORIEL 53682) with extinction of the laser light in the order of 10^{-6}. Fig. 18 shows the cryostat window during nitrogen deposition through a microwave discharge in one of the experiments at 20 K, with no warming being applied on the cryostat window.

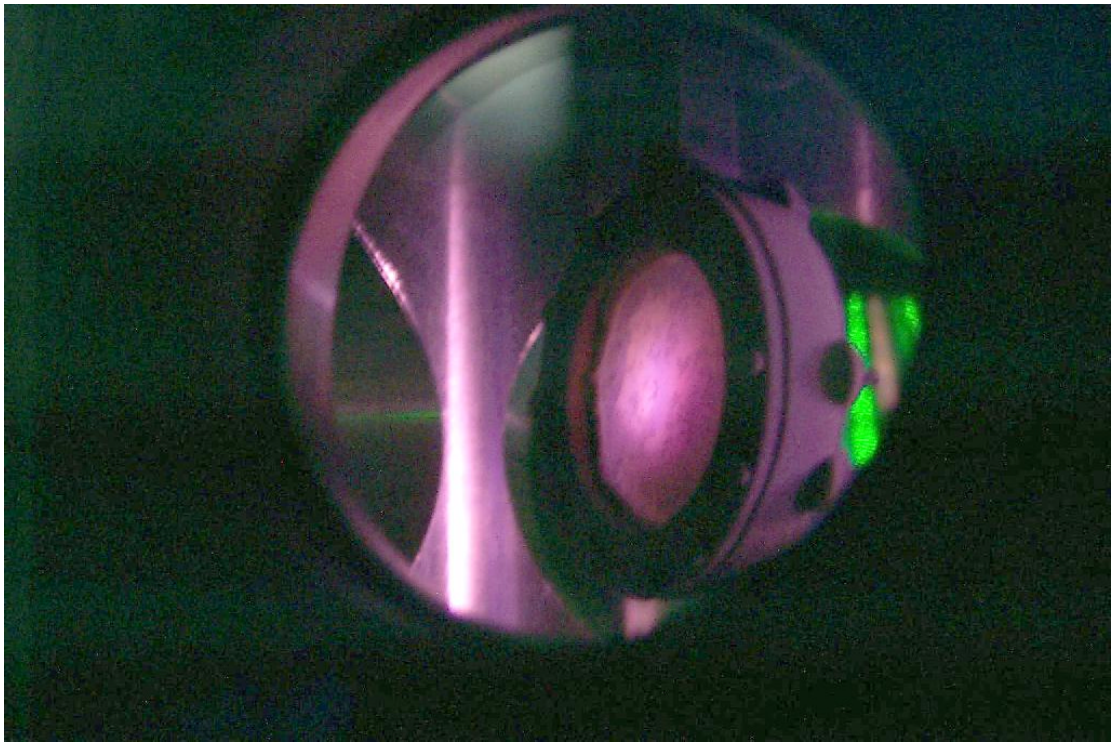

Fig. 18. The CRYOCOOLER cryostat window at 20 K during deposition of a 50/50 N_2/Ar mixture through a microwave discharge. The magenta color arises partly from nitrogen emission in the discharge tube (not shown). The green color is due to scattered light from the Ar^+ laser (blocked).

A few more experiments have been made studying the laser induced fluorescence previously reported [10] from matrices deposited through a microwave discharge. These bands have now been assigned as being due to residual plasma emission from the Ar^+ laser tube.

Calculations show that combination of two nitrogen molecules in the $A^3\Sigma_u^+$ state is favorable for the formation of N_4. A problem with this in an experimental approach is of course to obtain large enough population in the $A^3\Sigma_u^+$ state to make the process likely. If this could be achieved, however, this would be an alternative synthesis route to N_4. Therefore some attempts to optimize the concentration of molecules in the $A^3\Sigma_u^+$ state have been made. It has been found before [1] that α-particle bombardment of the matrix results in a high population of the v=0 level of the $A^3\Sigma_u^+$ state. It can be

argued that the population is still far too low to make the combination of two nitrogen molecules in the $A^3\Sigma_u^+$ state likely. However considering that the α-particles that create these nitrogen molecules in the $A^3\Sigma_u^+$ state will deposit their energy along a trace in the matrix, it is likely that these molecules are found next to each other. It may therefore be of interest to investigate this further.

Recent experiments with α-particle bombardment of the matrix have revealed that the intensity of the Vegard-Kaplan bands ($A^3\Sigma_u^+$- $X^1\Sigma_g^+$) is strongly dependent on the temperature (Fig. 19). The intensity curve may differ slightly in shape, but always seems to have a maximum intensity around 32 K and dies off to about the same intensity as in the 18 K matrix at about 37-38 K. The process is reversible. Since the mechanism is not yet known the reasons for this behavior cannot be proven, but it is reasonable to assume that the increase of intensity with increased temperature is due to the increased mobility of the molecules involved. It is also worth noticing that nitrogen has a phase transition at 37 K. A similar behavior has been reported by Savchenko et al. [15].

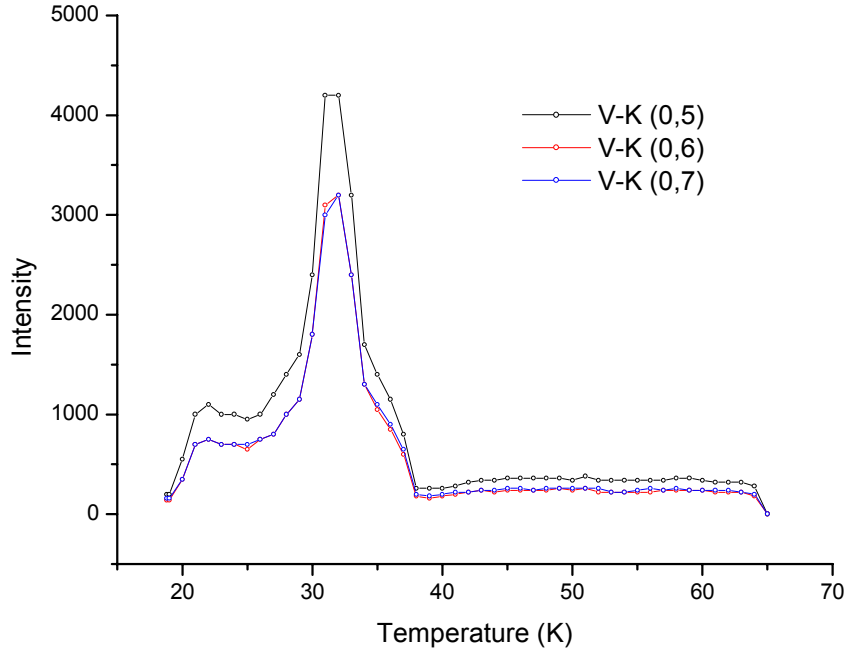

Fig. 19. The temperature dependence of the (0,5), (0,6) and (0,7) bands of the $A^3\Sigma_u^+$- $X^1\Sigma_g^+$ transition.

Bombarding the matrix with nitrogen ions from the AG 5000 ion gun also gives the Vegard-Kaplan bands under certain conditions. The bands are then very much stronger than what can be obtained with α-particle bombardment. The conditions under which the Vegard-Kaplan bands are strongest must be optimized. We have seen that a slight alteration of the experimental conditions may make the Vegard-Kaplan bands disappear completely in favor of other, yet unidentified, bands.

In future experiments we plan to put a filament near the matrix in order to spray the matrix with electrons and see whether this has any similar effects. We will also try to measure the true lifetime of the $A^3\Sigma_u^+$ state in the matrix. An accurate value is needed in order to be able to estimate the concentration of molecules in the $A^3\Sigma_u^+$ state. A preliminary estimate of the molar concentration, assuming that the lifetime is identical to the gas-phase value (1.9 s) gives a value of 10^{-8}, with an estimated inaccuracy of at least 1 order of magnitude.

We are not yet certain of the mechanism giving the $A^3\Sigma_u^+$- $X^1\Sigma_g^+$ transition. In order to optimize the concentration of molecules in the $A^3\Sigma_u^+$ state it is helpful to understand the process leading to it. Knowing if any higher energy transitions are present may help to do so. A VUV spectrometer has been set up for use with the CRYOCOOLER cryostat. This will be used to study whether any transitions from higher lying states than the $A^3\Sigma_u^+$ state are present during for example ion bombardment of the matrix.

Decomposition of high nitrogen content materials

Vapour deposition of 1H-5-t-butyl tetrazole onto a sapphire window.

Fine vapour deposited layers of 1H-5-t-butyl tetrazole and tetrazole/nitrogen mixtures have been deposited on a sapphire window in a cryostat for excitation and investigation with Raman techniques. The set-up allows for direct irradiation of the sample to take place while Raman spectra are being recorded. This will potentially allow for more dilute samples to be studied, giving insight into reaction mechanisms occurring during excitation.

Three methods were attempted to vapour deposit the 1H-5-t-butyl tetrazole onto the sapphire window: -

i) The sublimation of 1H-5-t-butyl tetrazole at room temperature at a pressure of 3-8x10^{-7} mbar onto a cold head at 12K. On leaving the sample for several hours the tetrazole appeared to have migrated from the sample holder into the main chamber. There was visible evidence of a white deposit on the copper cold head and also a build up of a white solid at the end of the stainless steel inlet tube leading from the sample chamber to the main chamber (Fig. 20). On analysing the deposit on the sapphire window using Raman spectroscopy the only signals observed were due to the impurities and the continuum of the sapphire window.

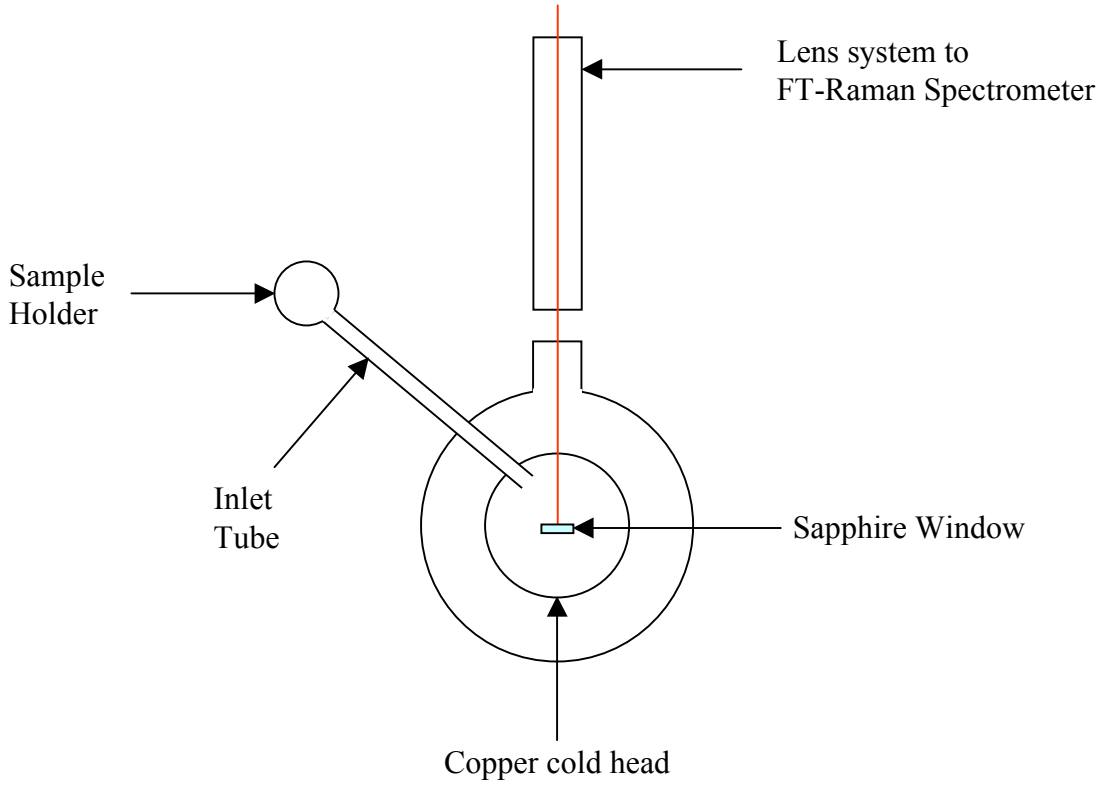

Fig. 20. Top view of the vapour deposition experimental set-up.

ii) Similar to the method above except that the external surfaces of the inlet system and the sample chamber were heated using heating tape. A temperature of 60°C was chosen. It was envisaged that thermal conduction through the metal surfaces would increase the rate of migration of the 1H-5-t-butyl tetrazole through the system and increase the amount of deposition onto the sapphire window. The rate of sublimation increased, as did the amount of white deposit observed on the copper cold head and at the end of the inlet tube however, the sapphire window showed no evidence of any deposited material.

iii) This method involved passing nitrogen gas through the heated sample to act as a carrier gas and a medium to trap the 1H-5-t-butyl tetrazole on the sapphire window. On passing the nitrogen through the sample for several hours a white deposit had formed over the cold head and the sapphire window. On examination of the deposit on the window using Raman spectroscopy a number of new signals were observed. Analysis of the spectrum assigned the signals as being due to oxygen impurity. The oxygen was introduced from a small leak in the gas chamber. There was no evidence of any 1H-5-t-butyl tetrazole trapped within the matrix.

The vapour deposition of the 1H-5-t-butyl tetrazole was proving to be more difficult than expected and owing to the time constraints on the attachment further efforts were not pursued.

Microwave irradiation of a pressed disk of 1H-5-t-butyl tetrazole in a copper holder was carried out. The sample was cooled to 12K and then irradiated for several minutes by a neon plasma. The sample was then analysed by Raman spectroscopy.

Initial spectra were dominated by black body radiation caused by the heating effect of the microwave radiation. As the sample and the surroundings cooled the black body radiation reduced and the spectra due to the sample dominated. On comparing the Raman spectra of the material before and after the microwave irradiation the spectra were identical and there was no evidence of any decomposition occurring. However on irradiation of the sample with the Raman YAG laser after the microwave irradiation did cause a broad band to appear in the region 3500-2250 cm^{-1} that may be caused by LIF of a very low concentration species which could not be detected under the conditions that were used.

Further work has to be carried out on these experiments to try to determine what species is giving rise to these emissions.

UV Decomposition Studies of high nitrogen content materials in a mass spectrometer.

As reported previously [17] initial investigations were being carried out on the decomposition of high nitrogen content materials using laser photolysis. A recently published Japanese Patent [13] reports the formation of a number of nitrogen species N_x (where x = 4,5,6,.., 10) by the decomposition of cyanuric azide using 355 nm UV photolysis in a mass spectrometer.

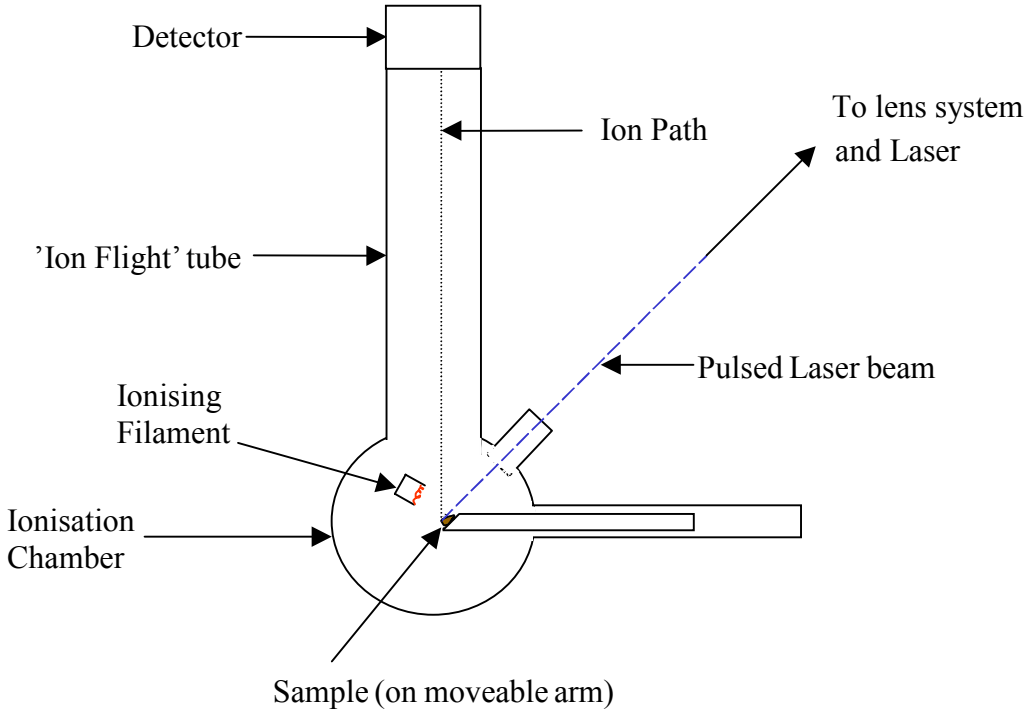

Fig. 21. Top view of the experimental set-up for the time of flight mass spectrometer decomposition experiments.

A time of flight spectrometer was used with a beam from a 355 nm YAG laser or a 308 nm excimer laser to photolyse the material (Fig. 21). In initial experiments, a CO_2 laser was also used. The products produced by the photolysis were then ionised by a filament and the corresponding ions detected by a dual multichannel plate detector with the output monitored using a LeCroy LC684DL 1.5 GHz oscilloscope. The output was analysed using either Excel or LabView routines.

Four materials have now been investigated, 1H-5-t-butyl tetrazole (1), π-cyclopentadienyl cobalt (1,4-dimethyltetraazadiene) (2), cyanuric azide (3) and N, N-dimethylaminophenyl pentazole (4). The results will now be discussed in more detail.

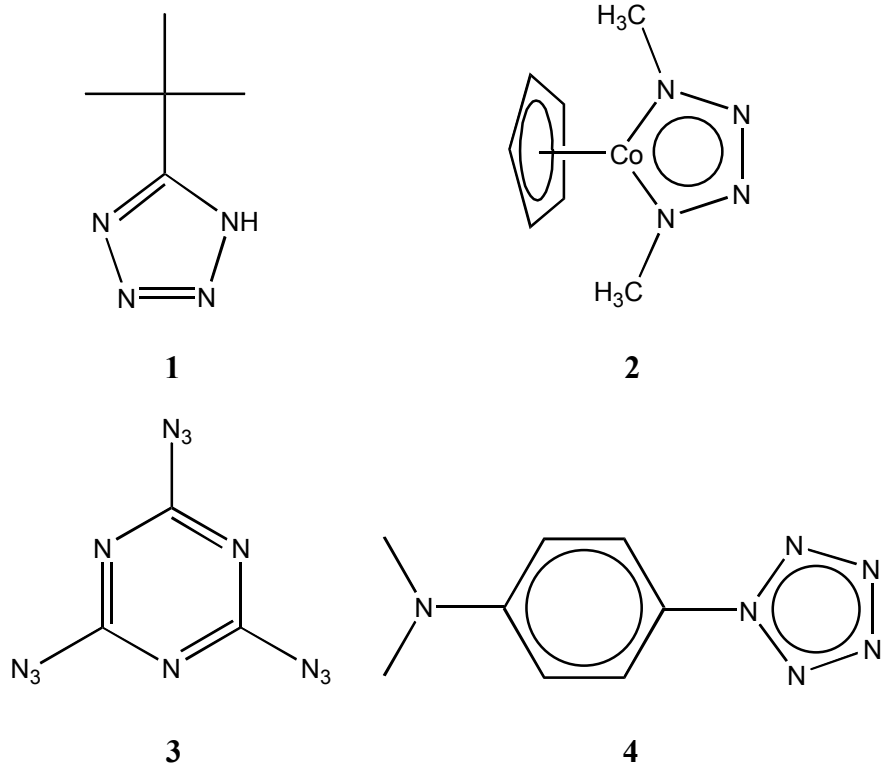

Fig. 22. The materials investigated using time of flight mass spectroscopy

Photolysis of 1H-5-t-butyl tetrazole

The tetrazole was investigated under a number of different conditions. The laser power, wavelength and exposure time were varied to determine whether the decomposition route of the material could be altered. The ionisation current was also altered to determine whether different fragmentation ions could be detected. Under all the conditions tried it was apparent that the decomposition of the tetrazole was following two potential routes; either a molecule of nitrogen was being split from the ring (Fig. 23, Pathway B) or hydrazoic acid was being cleaved off (Fig. 23, Pathway A).

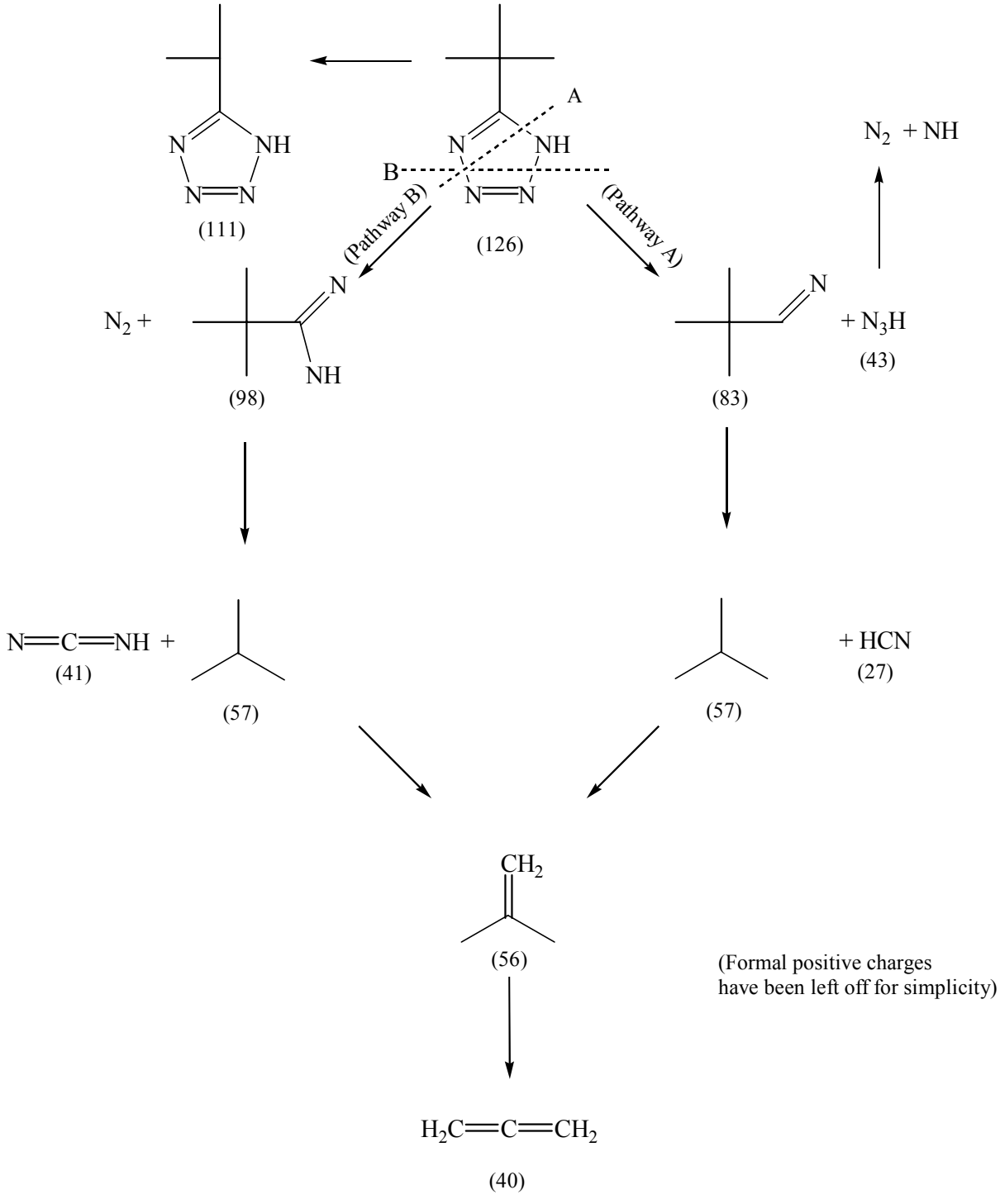

Fig. 23. Postulated fragmentation routes during the photolysis of 1H-5-t-butyl tetrazole.

Altering the laser power and wavelength had no great effect on the reaction pathway. On all the reactions carried out a molecular ion at 126 amu was never observed but a peak at 111 amu was observed. This corresponds to the loss of a methyl group from the t-butyl moiety. This is quite important, as this means that a C-C bond is breaking before either the N-N bonds in the cleavage of nitrogen molecule or the N-N and C-N bonds if hydrazoic acid is cleaved. However, the formation of a N_4 derivative (linear, square planar or tetrahedral) by the systematic cleavage of bonds would require the breaking of a C-N double bond before the breaking of a single nitrogen bond.

Photolysis of π-cyclopentadienyl cobalt (1,4-dimethyltetraazadiene)

This material was studied as it had four nitrogen atoms linked in a row. It was also envisaged that the possibility of cleaving off the end methyl groups would be possible with the nitrogen atoms being stabilised by the metal centre.

Initial studies were carried out on the material without photolysis to determine the normal mode of fragmentation (Fig. 24).

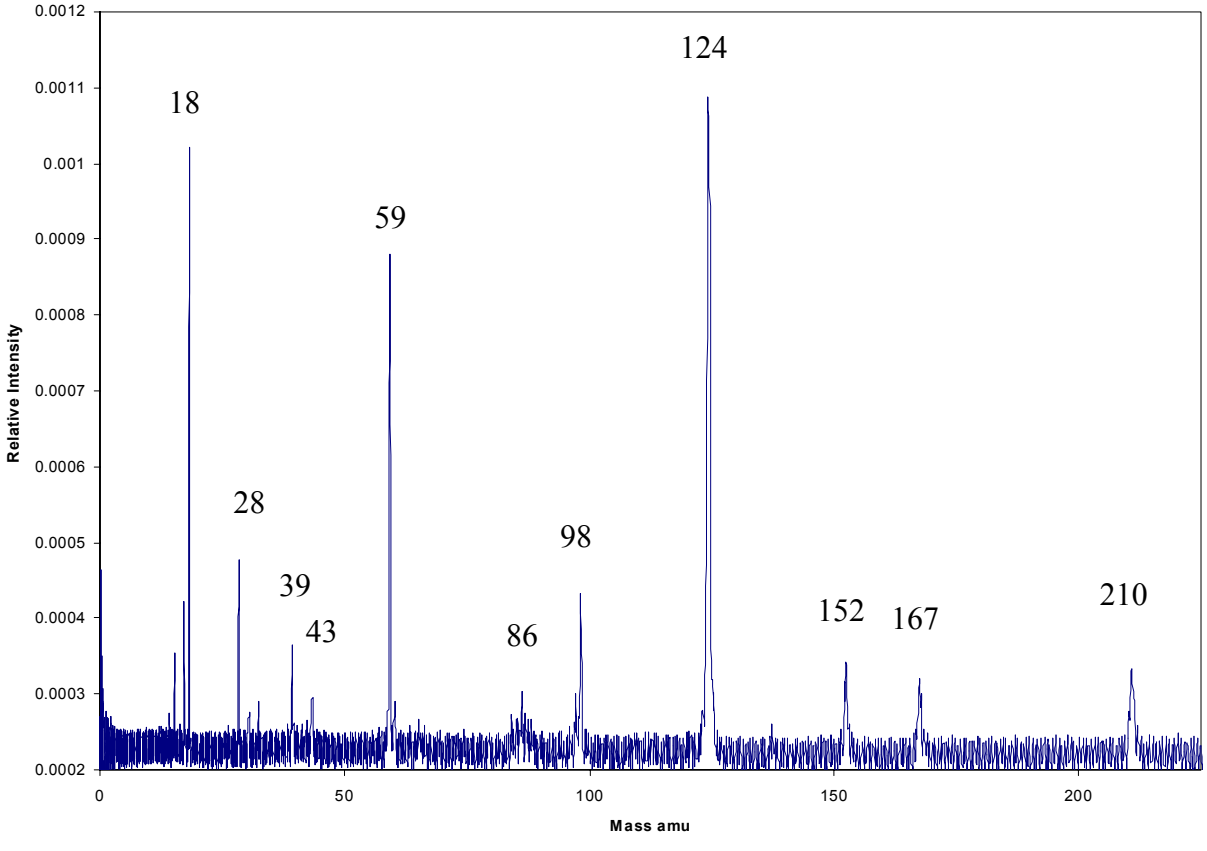

Fig. 24. Mass spectrum of cyclopentadienyl cobalt 1,4-dimethyltetraazadiene prior to photolysis

The material appeared to follow two potential pathways (Fig. 25) with pathway A being predominant. Pathway A involves the initial loss of azomethame (CH_3N_2). The resulting 'azomethane' metal complex then loses a methyl group to give a dinitrogen metal complex. Pathway B involves the initial loss of dimethyltetraazadiene from the complex as a small metastable peak is observed at 86 amu. An alternative source for this peak is the recombination of two azomethane fragments. The stability of the cobalt cyclopentadienyl fragment is quite apparent with the peak at 123 amu having the greatest intensity. There was no evidence of the cyclopentadienyl ring being cleaved off leaving the cobalt tetrazene complex. The remaining peaks can be attributed to the decomposition of the cyclopentadienyl cobalt complex.

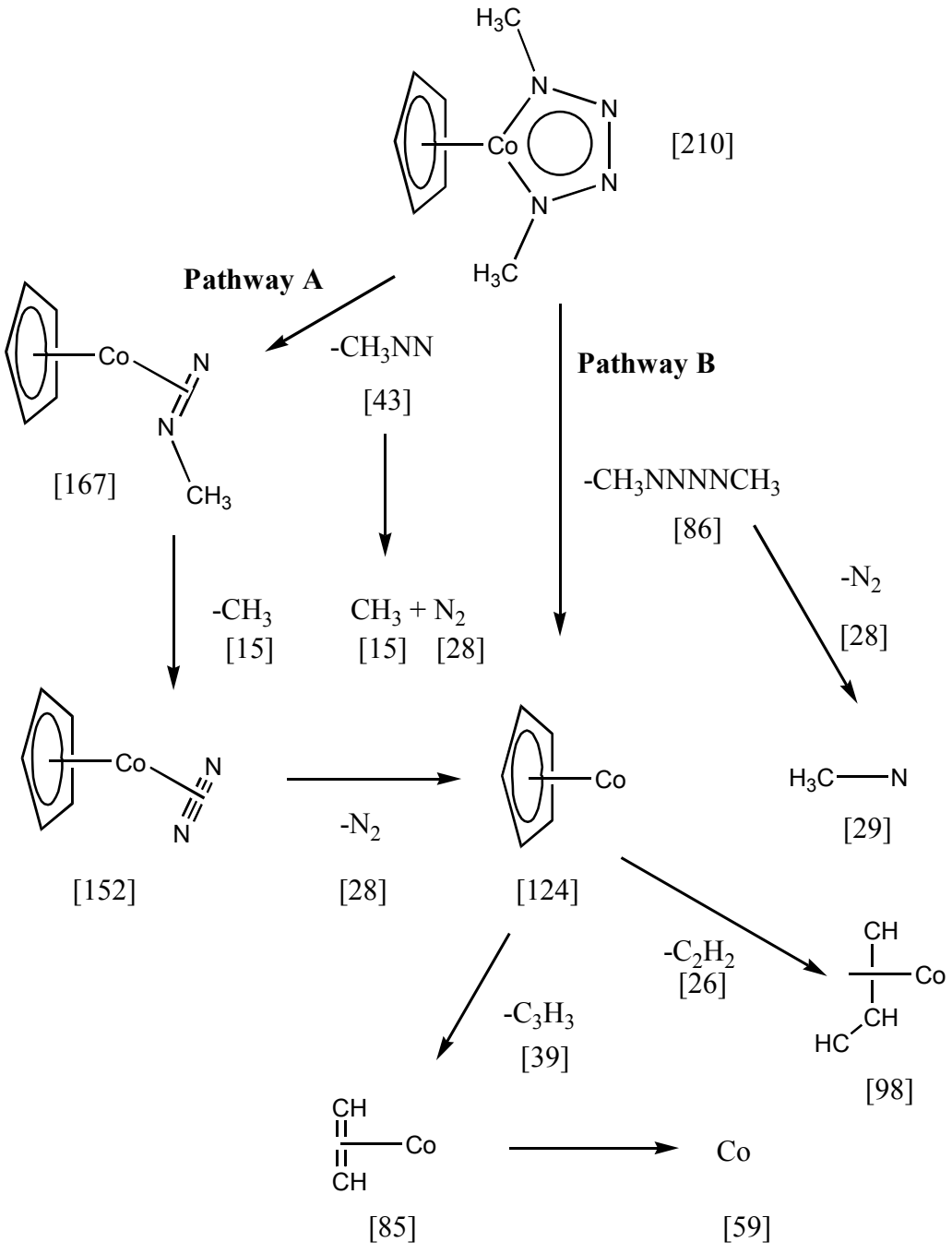

Fig. 25. Postulated fragmentation routes during the photolysis of cyclopentadienyl cobalt 1,4-dimethyltetraazadiene

On irradiating the sample brought about two major effects, i) that a lot more sample was volatilised and ii) greater fragmentation was observed (Fig. 26).

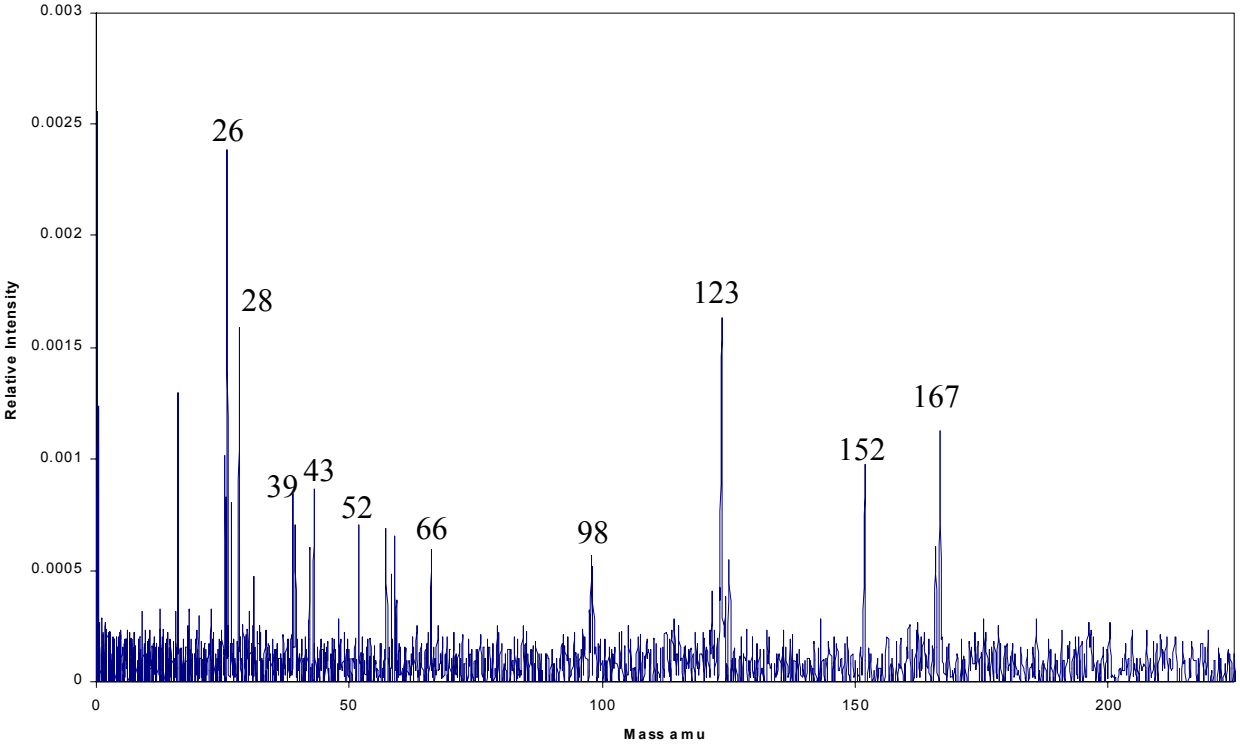

Fig. 26 Mass spectrum from the photolysis of cyclopentadienyl cobalt 1,4-dimethyltetraazadiene

Although the spectra were more complex the general mechanism of fragmentation appeared to be the same but it has not been possible to assign all the signals. However, some spectra gave totally different fragmentation patterns and these have not been explained.

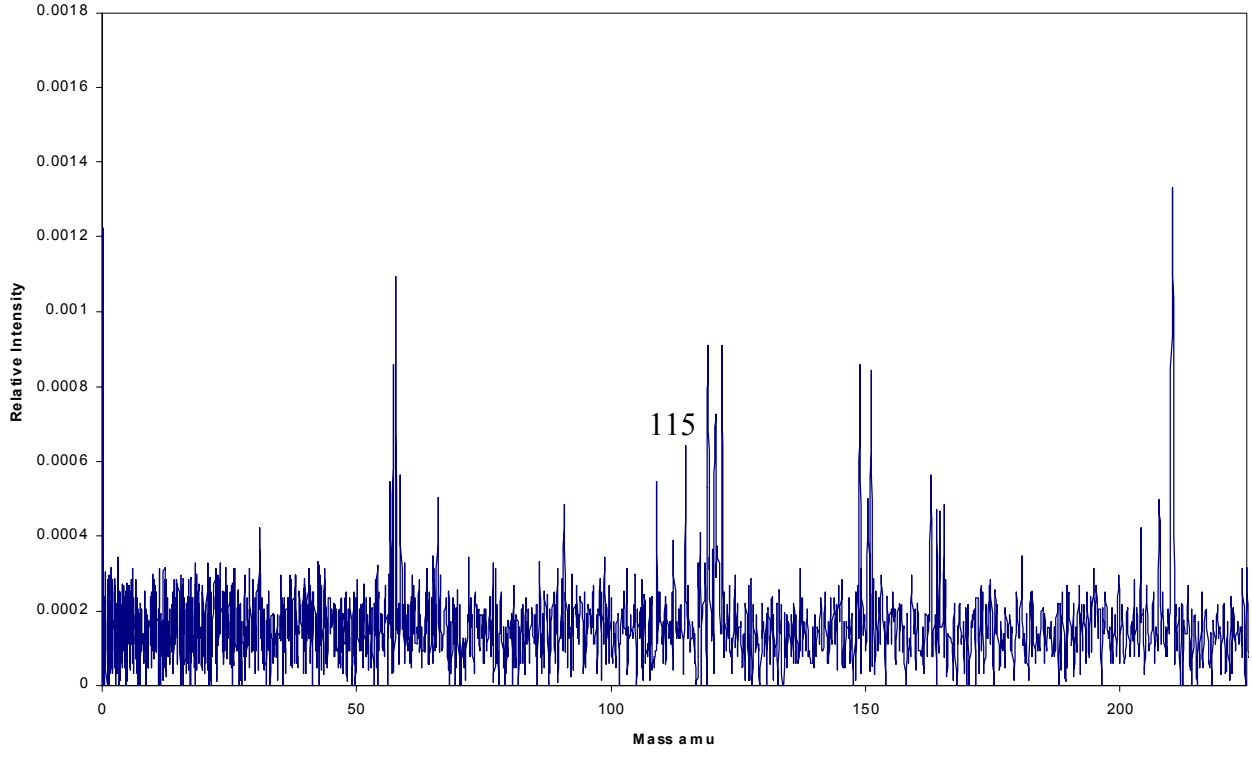

Fig. 27 Mass spectrum of cyclopentadienyl cobalt 1,4-dimethyltetraazadiene with a peak at 115 amu, possibly corresponding to CoN_4

The spectrum (Fig. 27) is quite noisy but the interesting feature of the spectrum is a peak at 115 amu that may correspond to CoN_4. However, caution must be exercised, as there is no evidence of any peaks at 56, 42, or 28 amu corresponding to the fragmentation pattern that might be expected for N_4.

Photolysis of Cyanuric Azide

A recent patent [13] claims to have prepared a number of nitrogen allotropes by the laser decomposition of cyanuric azide. We therefore tried to repeat their work. However, the patent does not describe any of the experimental conditions or the parameters that were used.

Cyanuric azide was studied under a number of conditions but results comparable to those attained by the Japanese workers were never obtained. In a majority of the experiments similar spectra were observed (Fig. 28) and a possible fragmentation scheme is shown in Fig. 29. This differs from the Japanese work where they observe fragmentation signals at 162 amu corresponding to the loss of a single azide group. This was never observed in our studies.

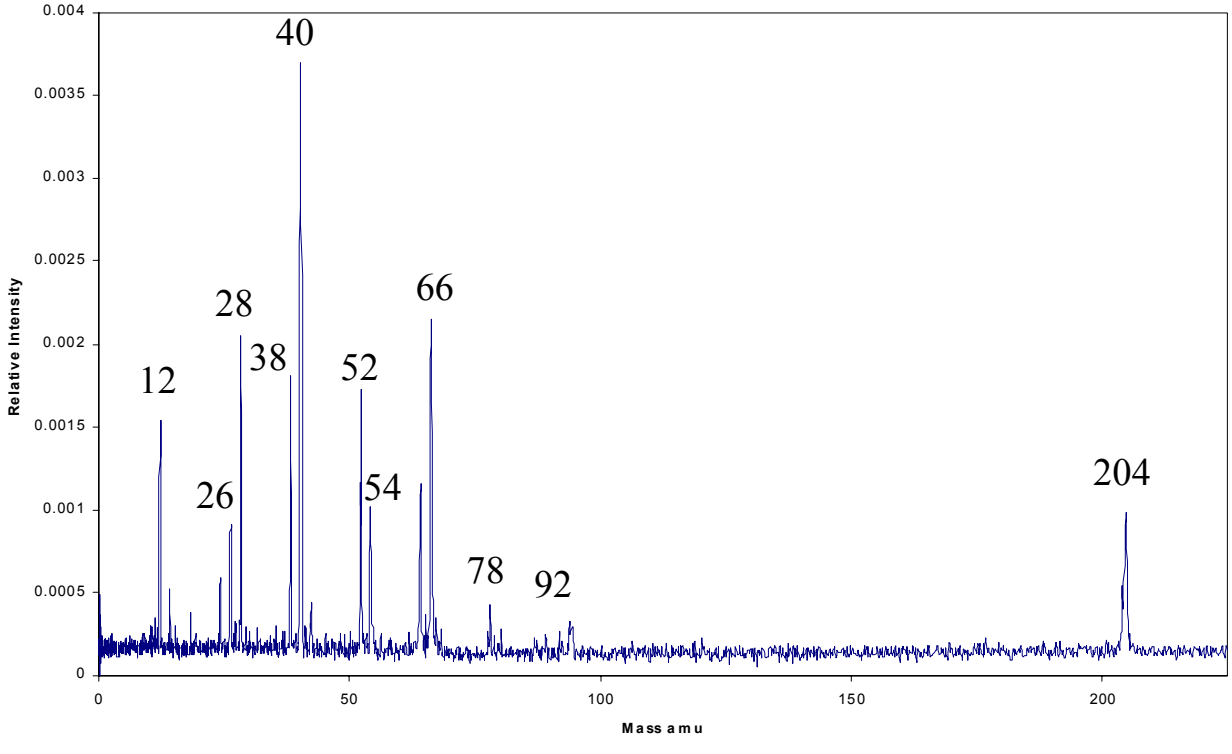

Fig. 28. Mass spectrum from the photolysis of cyanuric azide

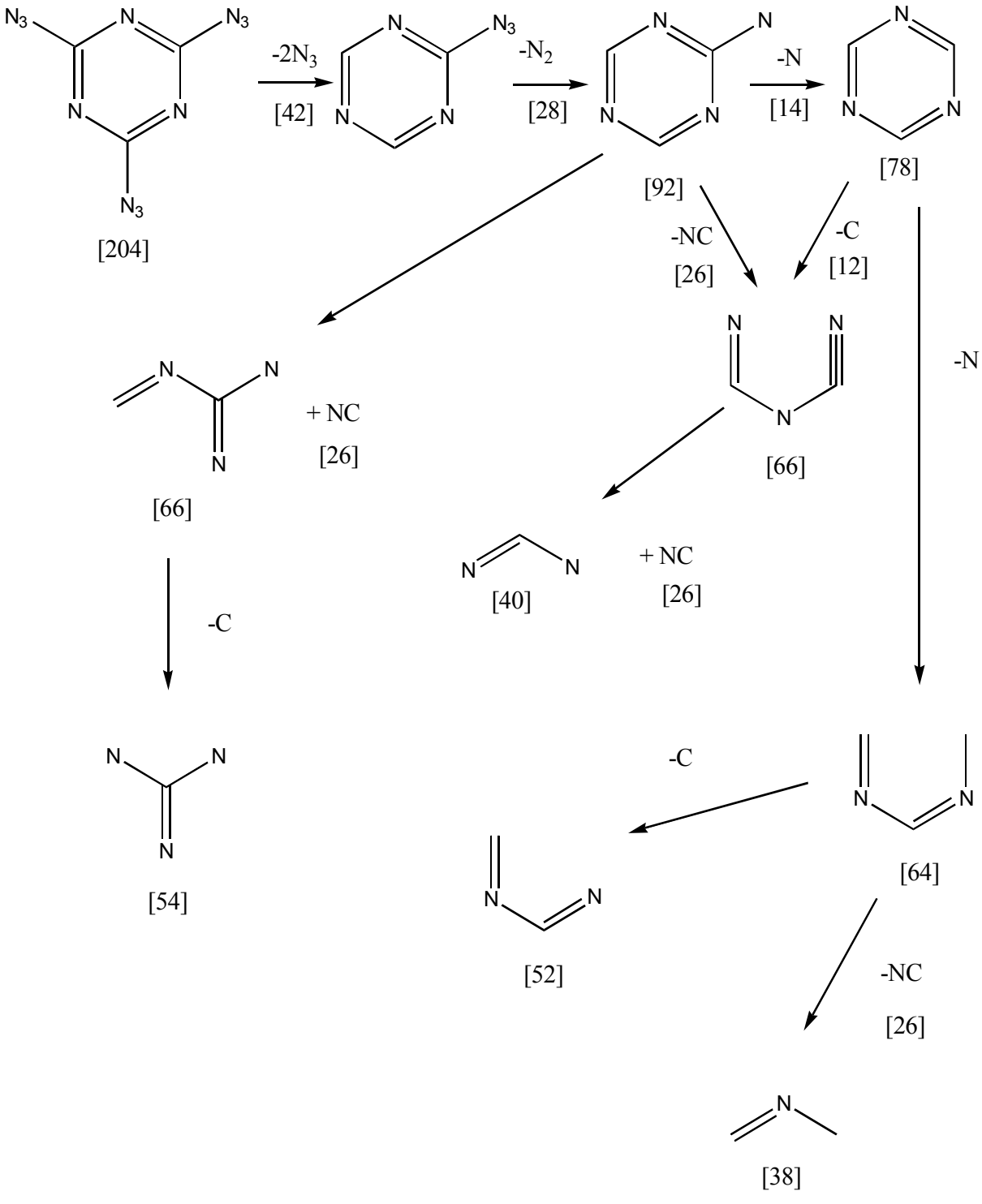

Fig. 29. Postulated fragmentation routes during the photolysis of cyanuric azide

More importantly no signals were observed at 56, 70 or 140 amu which would correspond to N_4, N_5 and N_{10} respectively. This however, may be expected as during our studies we were looking at the entire product range of the materials. We do not envisage that the new nitrogen allotropes are going to be present in very high concentration so a better technique would be to use a gated mass spectrometry system where mass-selected ions can be studied. It is possible that the above nitrogen allotropes are present but they are in too low a concentration to be observed. Using the gated approach it would be possible to analyse the ions by mass spectrometry and by further minor modifications of the apparatus it would be possible to trap out the ions on a cold surface and analyse them using other techniques such as Raman spectroscopy.

Photolysis of N, N-dimethylaminophenyl pentazole.

Initial investigations were carried out on this material to determine whether the pentazole (70 amu) or the dimethylaminophenyl (120 amu) mass fragments could be observed.

Initial results indicate that neither the pentazole nor the dimethylaminophenyl fragments are observed in the mass spectrum (Fig. 30).

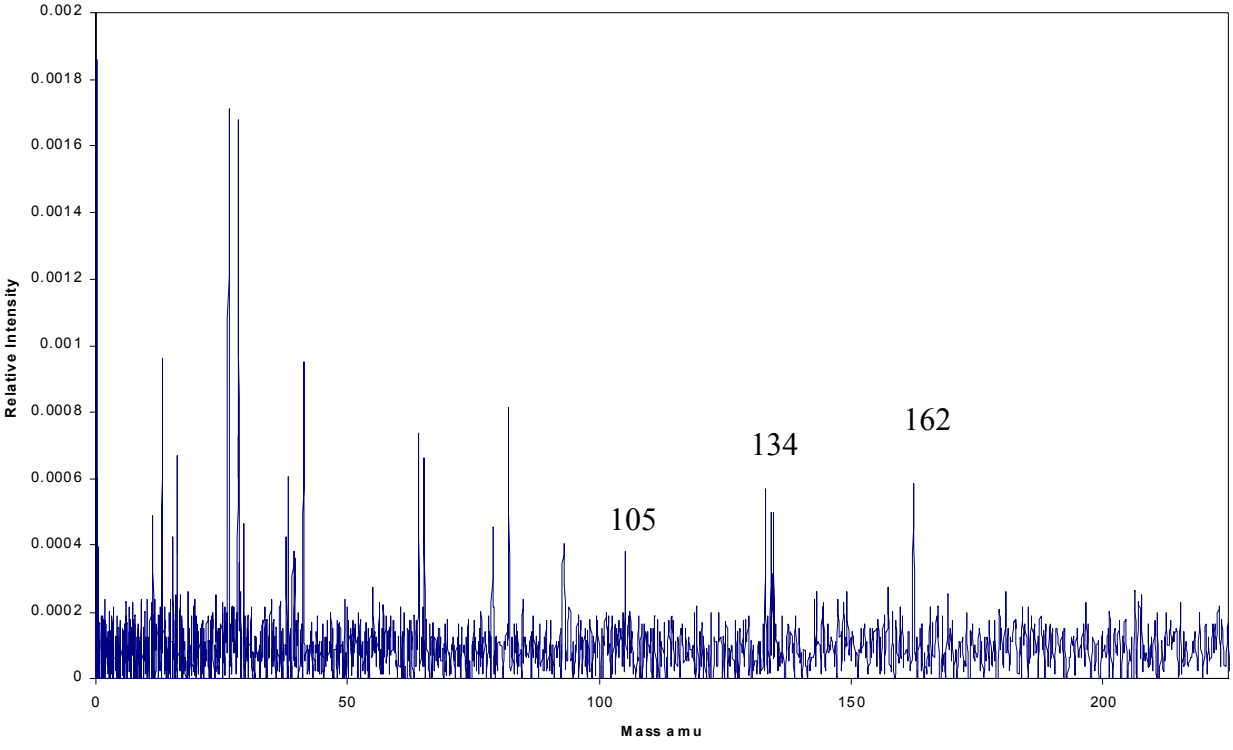

Fig. 30. Mass spectrum from the photolysis of N,N-dimethylaminophenylpentazole

Rather, initial loss of nitrogen (N_2) followed by a second, giving rise to the peaks at 162 and 134 amu respectively. The fragmentation that then follows appears to involve some complex rearrangements and this has not been fully characterised. However, it was noticed that the mode of fragmentation could be altered and it may be possible to alter the ion fragments formed.

It is important to note that the work carried out was done using a positive ion detector. It may therefore not be surprising that the pentazole fragment was not observed, as the pentazole cation is not stable. However, if a negative detector were used then the probability of observing the pentazole anion would be greatly increased due to its stability.

SERS experiments

As has been pointed out in several occasions, the inherently low cross-section of Raman scattering presents a formidable problem for the detection of $N_4(T_d)$ with Raman techniques. For this reason, we are trying to apply Surface Enhanced Raman Spectroscopy (SERS) to lower the detection limit. It is well-documented that huge Raman enhancement factors (typically 10^6) are achievable in the case of many organic molecules on prepared silver surfaces. Whether of not such factors are achievable in the case of small inorganic molecules at cryogenic temperatures is an entirely different matter, however. A strong wavelength dependence of the SERS efficiency might also be present, possibly causing SERS to be less attractive in the infrared.

We have prepared SERS-active silver surfaces using electrochemical roughening procedures, estimated the surface quality using an electron microscope (Jeol JSM-6400), and performed calibration experiments on previously known substances, such as adenine, pyridine, benzene, N_2O and P_4. All SERS-active surfaces were prepared by an electrochemical etching method, similar to that described by Roth et al. [16]. However, we used slightly higher voltages for the reduction-oxidation cycles. In our experiments, the working electrode was pre-reduced at 2.0 V for 5 minutes before being subjected to four alternating cycles of ± 1.0 V of 30 seconds each (4 minutes in total).

A typical example of SEM-picture of a SERS-active silver surface is shown in Fig. 31. Test spectra of adenine are shown in Figs. 32 and 33.

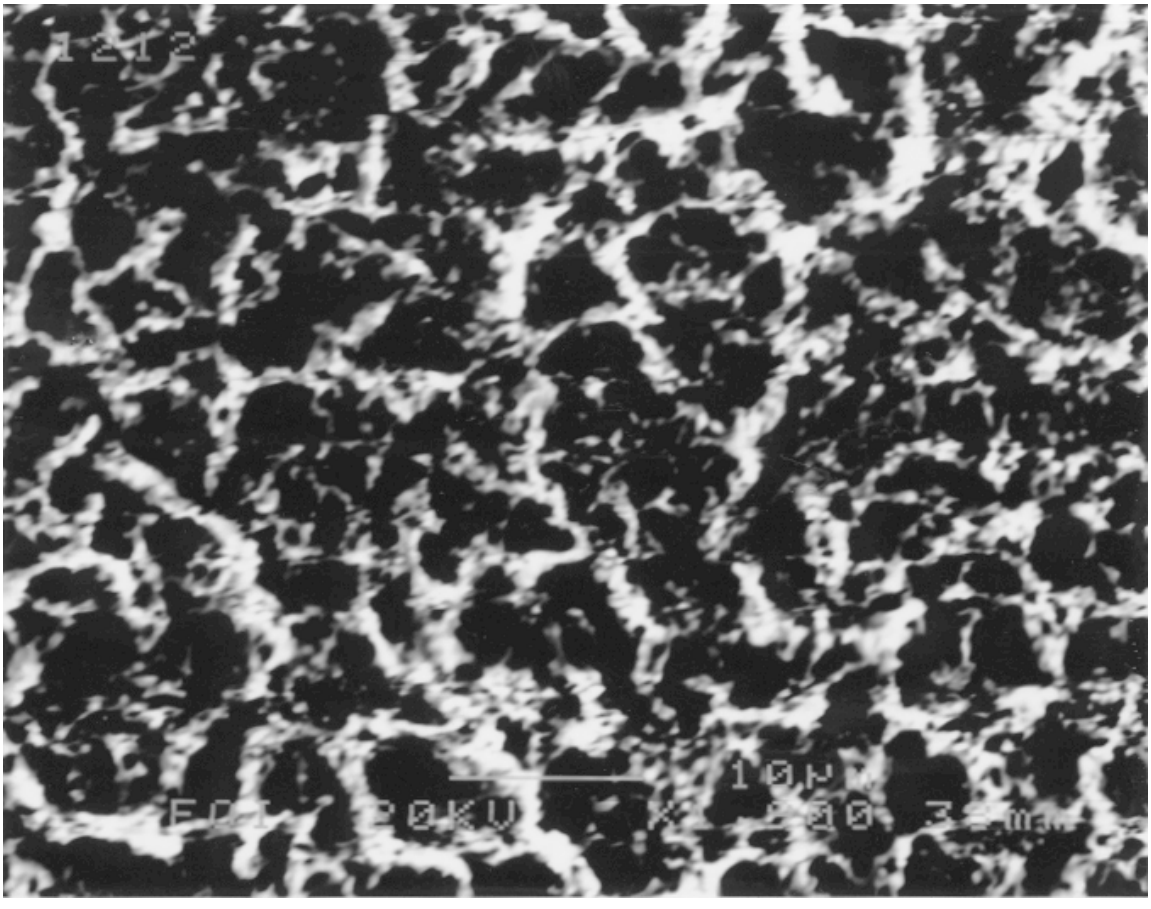

Fig.31. A 55 x 43 μ portion of an electrochemically activated silver surface, used in the SERS experiments.

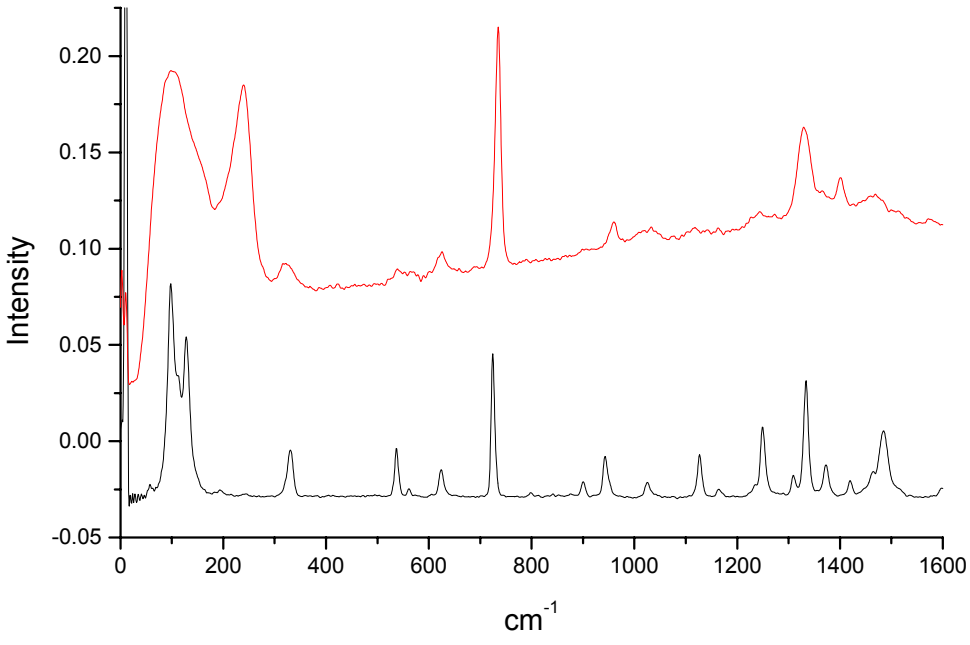

Fig. 32 *Upper trace:* Raman spectrum of adenine, deposited on electrochemically roughened silver surface. *Lower trace:* Raman spectrum of adenine sample in a capillary tube. The number of interrogated molecules is orders of magnitude larger in the lower spectrum. Both spectra were recorded without the intermediate lens system, using a 16 mm objective. 300 scans/spectrum, laser power = 300 mW. Resolution = 4 cm^{-1}.

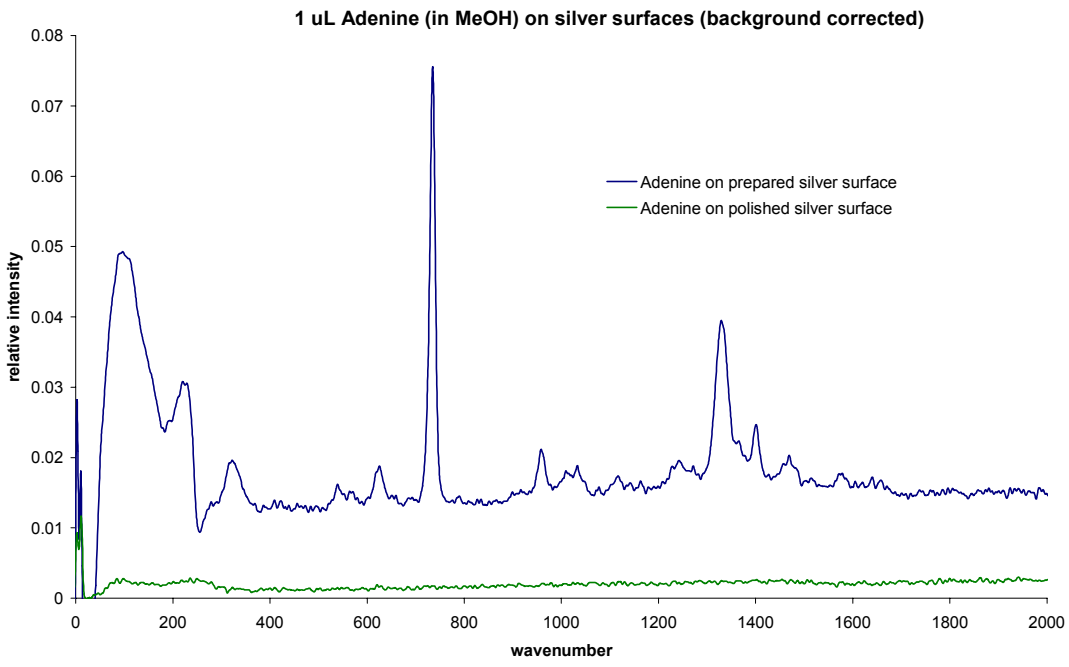

Fig. 33. *Upper trace:* Raman spectrum of adenine on electrochemically roughened silver surface. *Lower trace:* Raman spectrum of adenine on untreated silver surface. The spectra were recorded in otherwise identical conditions, except for the surface quality. Both spectra were recorded without the intermediate lens system, using a 16 mm objective. The SERS enhancement obviously amounts to several orders of magnitude. 300 scans/spectrum, laser power = 300 mW. Resolution = 4 cm^{-1}.

We have also carried out SERS experiments on some inorganic substances, e.g. N_2O and P_4. In the case of P_4, we observed an inherently strong (not SERS-enhanced) Raman signal. A typical spectrum is shown in Fig. 34. In this spectrum, the three vibrational modes $\nu_1(A_1)$, $\nu_2(E)$ and $\nu_3(F_2)$ are clearly resolved.

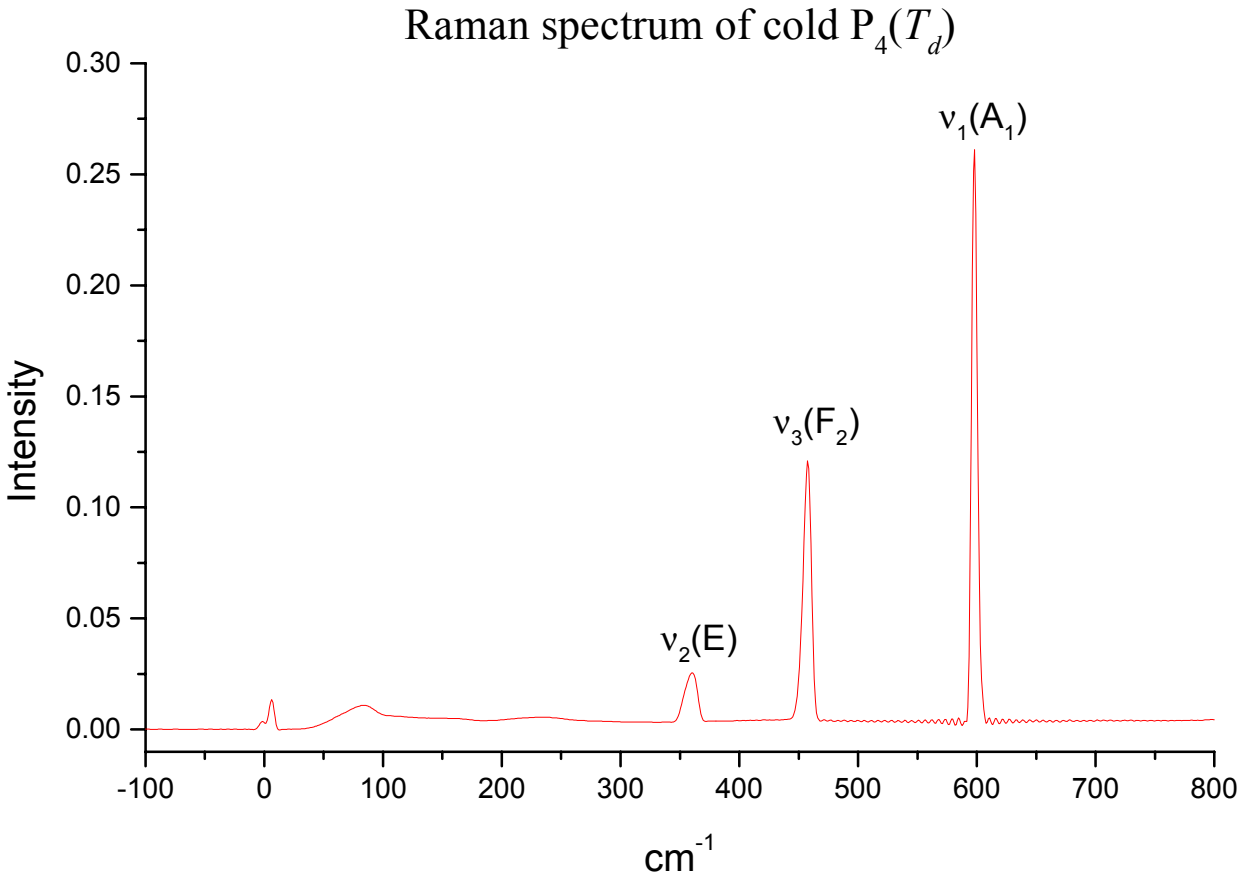

Fig. 34. A Raman spectrum of solid P_4, deposited on silver surface at 15 K. The measured wavenumbers for the three modes are 359.8 cm^{-1} [$\nu_2(E)$], 457.5 cm^{-1} [$\nu_3(F_2)$] and 598.5 cm^{-1} [$\nu_1(A_1)$]. Laser power = 400 mW. In total, 5100 scans were recorded at a resolution of 4 cm^{-1}.

Warming-up experiments were subsequently performed on the P_4 samples. In the Raman spectra shown in Fig. 35, the temperature was gradually increased from 15 K to 240 K. In the temperature interval between 100 K and 180 K, additional lines appeared in the 50-100 cm^{-1} region. At the same time, the intensities of the three P_4 Raman lines decreased temporarily. This indicates that a molecular rearrangement is taking place in this temperature interval. The phenomenon is being further investigated at present.

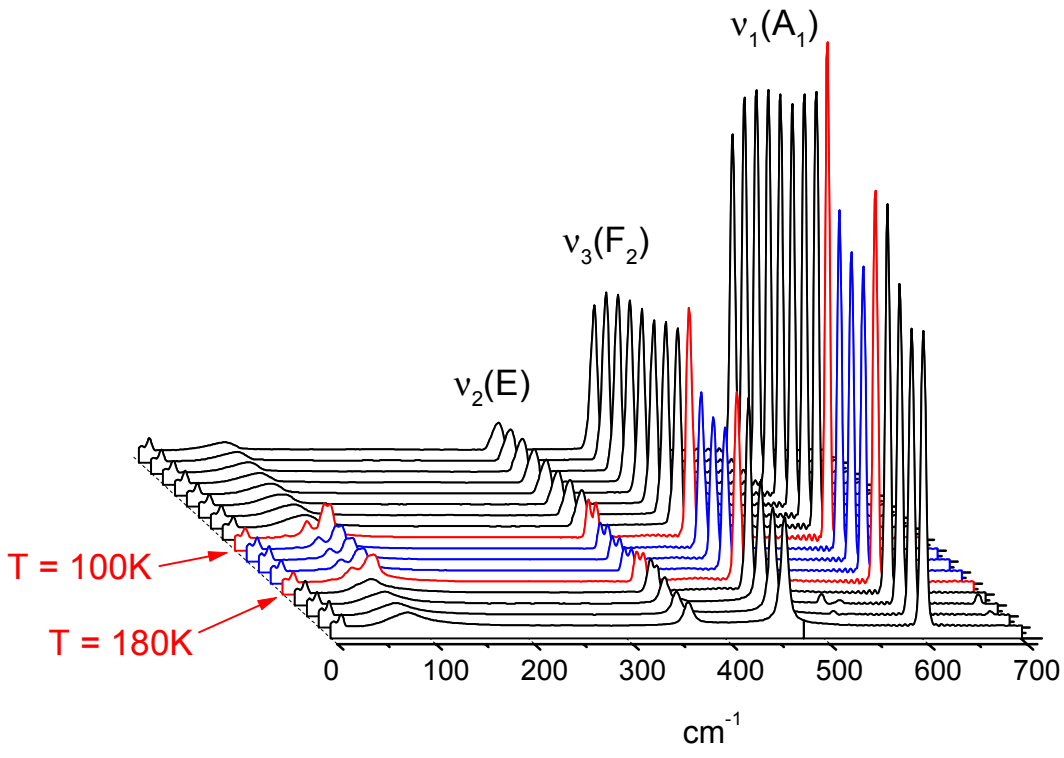

Fig. 35. A warm-up series of P_4, deposited on electrochemically roughened silver surface. A rearrangement of the crystal obviously occurs in the interval between 100 K and 180 K. However, the molecular symmetry seems to be strictly T_d both for T < 100 K and for T > 180 K. Laser power = 400 mW, 300 scans/spectrum. Resolution = 4 cm^{-1}.

We have calculated frequencies and Raman activities for $P_4(T_d)$ at two different levels (B3LYP/6-31G(d) and B3LYP/6-311G(d)). The results are summarized in Table 1.

Table 1. A comparison of calculated and experimental data on $P_4(T_d)$. The values marked with asterisks are experimental intensities in arbitrary units, where total peak areas in Fig. 34 have been used as intensity measure. Note that the experimental intensities are reproduced almost perfectly by the B3LYP/6-311G(d) calculations.

	B3LYP/6-31G(d)	B3LYP/6-311G(d)	Experiment
$\nu_1(A_1)$ frequency (cm^{-1})	607.2	598.6	598.5
$\nu_1(A_1)$ Raman act. ($Å^4u^{-1}$)	63.0	79.0	80*
$\nu_2(E)$ frequency (cm^{-1})	367.6	360.1	359.8
$\nu_2(E)$ Raman act. ($Å^4u^{-1}$)	34.2	17.6	18*
$\nu_3(F_2)$ frequency (cm^{-1})	464.2	453.3	457.5
$\nu_3(F_2)$ Raman act. ($Å^4u^{-1}$)	69.8	57.5	54*

Theoretical calculation of the density of N_4

For theoretical estimates of the density of N_4, the program MOLPAK (MOLecular PAcKing) from University of Maryland [8] has been used. MOLPAK uses the calculated electrostatic potential surfaces from Gaussian 98 at the B3LYP/6-31G(d) level as a starting-point for the molecules to be packed. MOLPAK uses group theory to pack the molecules in 29 different space groups and the minimum energy is calculated for each space group. The space group which gives the lowest energy is considered as the most probable packing and the corresponding density is the estimated theoretical density. The MOLPAK program has not been written for pure nitrogen clusters, so there is an uncertainty in the prediction of the density. Especially for $N_4(D_{2h})$ one can choose between four different orbital bondings (atom code volume additivity). A more thorough evaluation of the space groups would lead to more accurate results.

Molecule	**Density (g/cm^3)**
$N_4(T_d)$	2.26
$N_4(D_{2h})$	2.17 – 2.62

The resulting calculated densities, extracted from MOLPAK's output data.

Theoretical studies on excited states of N_4

Parallel to the experimental work, theoretical studies have been performed with the objective to provide information that can aid the synthesis efforts. In an earlier study [3] we investigated the triplet N_4 potential energy surface using density functional theory (DFT) and high level *ab initio* methods, e.g. CASSCF, MRCI, and CCSD(T). We discussed the stability of the stationary points relative to the tetrahedral form of N_4. In particular, one stable triplet isomer of N_4 of D_{2d} symmetry was identified and characterized, and it was concluded that this isomer is likely to be an intermediate in synthetic routes which involve the formation of N_4 (T_d) from triplet excited states of N_2.

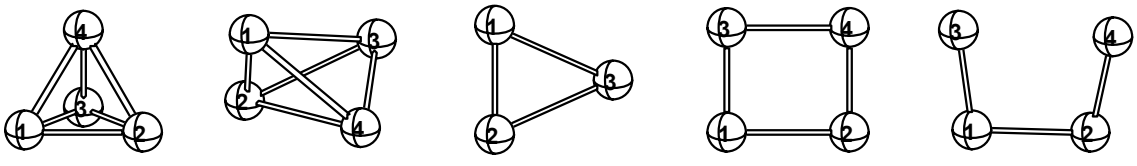

Fig 36. Optimized structure of stationary points discussed in this report in order of appearance.

One focal point of the continued work has been to identify alternative methods of detecting the N_4 isomers. We have previously determined the IR and Raman spectra of the two N_4 isomers and estimated their detection limits in Raman spectroscopy [4]. However, even with the use of high power lasers the detection limits for Raman spectroscopy are relatively high. Laser-induced fluorescence (LIF) is a much preferred method due to its higher sensitivity. In order to identify possible transitions to be used in LIF spectroscopy, the vertical electronic excitation energies for the lowest 11 singlet states of N_4 (T_d) were evaluated using time dependent DFT with the B3LYP functional and using EOM-CCSD (equation-of-motion CCSD) theory [6]. The EOM-CCSD/d-AVDZ calculations predict that there are two optically accessible singlet

states of T_2 symmetry at 10.26 eV and 10.56 eV. These transitions are relatively weak. The transition to the third T_2 state, which is predicted to lie 10.65 eV above the N_4 (T_d) ground state, is stronger by about one order of magnitude. However, this state is still hard to reach using one-photon absorption, since the low excitation wavelength precludes the use of a high-power laser as the radiation source. We have therefore calculated the two-photon transition probabilities for excitation to the lowest lying states of N_4 (T_d) using the quadratic response CCSD (QR-CCSD) theory. The results from our calculations of both one-photon oscillator strengths and two-photon absorption probabilities are summarized in Table 2. It can be seen that some states that are one-photon dipole-forbidden are two-photon allowed, e.g. this is the case for the ^1E and $^1A_1$ states. However, for both one-photon and two-photon transitions the 3^1T_2 state is the most active. Since the ground state N_4 (T_d) molecule is strongly bound and, since the transition to the 3^1T_2 state is of Rydberg character, we believe this state to be bound. This fact together with the sizeable two-photon absorption probability is likely to make the 3^1T_2 state useful for detection by LIF spectroscopy.

Table 2. EOM-CCSD/d-AVDZ vertical excitation energies (ΔE_{vexc}) (in eV) and one photon oscillator strengths (*f*), and QR-CCSD/d-AVDZ two-photon transition probabilities (TPA) (in atomic units) for N_4 (T_d).

State	ΔE_{vexc}	*f*	TPA
1^1T_1	9.65	0.0	0.0
1^1T_2	10.26	0.0336	0.761
1^1E	10.28	0.0	15.818
2^1T_1	10.30	0.0	0.0
2^1T_2	10.56	0.0005	0.083
3^1T_1	10.60	0.0	0.0
3^1T_2	10.65	0.1974	253.6
4^1T_1	10.67	0.0	0.0
1^1A_1	10.75	0.0	12.44

Mass spectrometry with ion-detection may be an alternative method for detecting N_4 (T_d). However, this method requires that the formed N_4^+ cation is sufficiently stable to survive until detection. We have therefore investigated the tetrahedral region of N_4^+ potential energy surface. A stable D_{2d} minimum ($^2A_2$), which is slightly distorted from T_d symmetry, has been identified. The structural parameters, vibrational frequencies and ionization potentials are collected in Table 3.

Table 3. Equilibrium structure (Å, deg), harmonic frequencies (cm^{-1}), for N_4^+ (D_{2d},$^2A_2$), and the adiabatic ionization potential (eV) for N_4(T_d).

Method	R_{12}	R_{13}	α_{123}	$\omega_1(b_1)$	$\omega_2(e)$	$\omega_3(a_1)$	$\omega_4(b_1)$	$\omega_5(a_1)$	IP_{adiab}
CAS(12,11)/VTZ	1.295	1.686	67.4	362	543	570	1131	1371	
CCSD(T)/ VTZ	1.289	1.679	67.4						12.37

The energy of the N_4 (T_d) molecule relative to two N_2 molecules has been estimated to be 183 kcal/mol from CCSD(T)/VTZ calculations. This large energy difference makes it difficult to synthesize N_4 (T_d) using N_2 molecules as the reactants. We have therefore investigated the possibility of making N_4 (T_d) from nitrogen atoms and N_3 radicals. Electronically excited nitrogen atoms (^{2}D, ^{2}P) can be generated in a cryogenic environment. A suitable N_3 radical should have an appropriate geometrical configuration of the atoms in order to facilitate the generation of N_4 (T_d). The ground electronic state of the N_3 radical has a linear form and is not likely to be suitable for formation of N_4 (T_d). We have studied some other N_3 isomers hitherto not reported experimentally at various computational levels. These calculations indicate that a stable ring N_3 (C_{2v}) isomer should exist with a $^2B_1$ electronic state. This isomer has similar bond lengths and bond angles as N_4 (T_d), which indicates that it can be a suitable precursor for the N_4 (T_d) synthesis according to the scheme: $N_3(^2B_1)+N(^2D)\rightarrow N_4(^1A_1)$. Vibrational frequencies, IR and Raman intensities that can be useful for the detection of N_3 (C_{2v}) are presented in Table 4.

Table 4. Equilibrium structure (Å, deg), harmonic frequencies (cm^{-1}), zero point energy (kcal/mol), energy difference (eV), IR and Raman intensities (km/mol) for the ring N_3 (C_{2v},$^2B_1$) radical.

Method	R_{13}	R_{12}	α_{132}	$\omega_1(b_2)$	$\omega_2(a_1)$	$\omega_1(a_1)$
CAS(15,12)/ **VTZ**	1.483	1.232	49.1	285	826	1632
B3LYP/ **AVDZ**	1.457	1.229	49.9	351 [12.88][a] (13.56)[b]	905 [0.24][a] (13.46)[b]	1729 [4.19][a] (27.13)[b]
CCSD(T)/ **AVDZ**	1.478	1.247	49.9	510 [5.62][a]	859 [0.56][a]	1631 [3.77][a]

[a] IR intensities, [b]Raman intensities

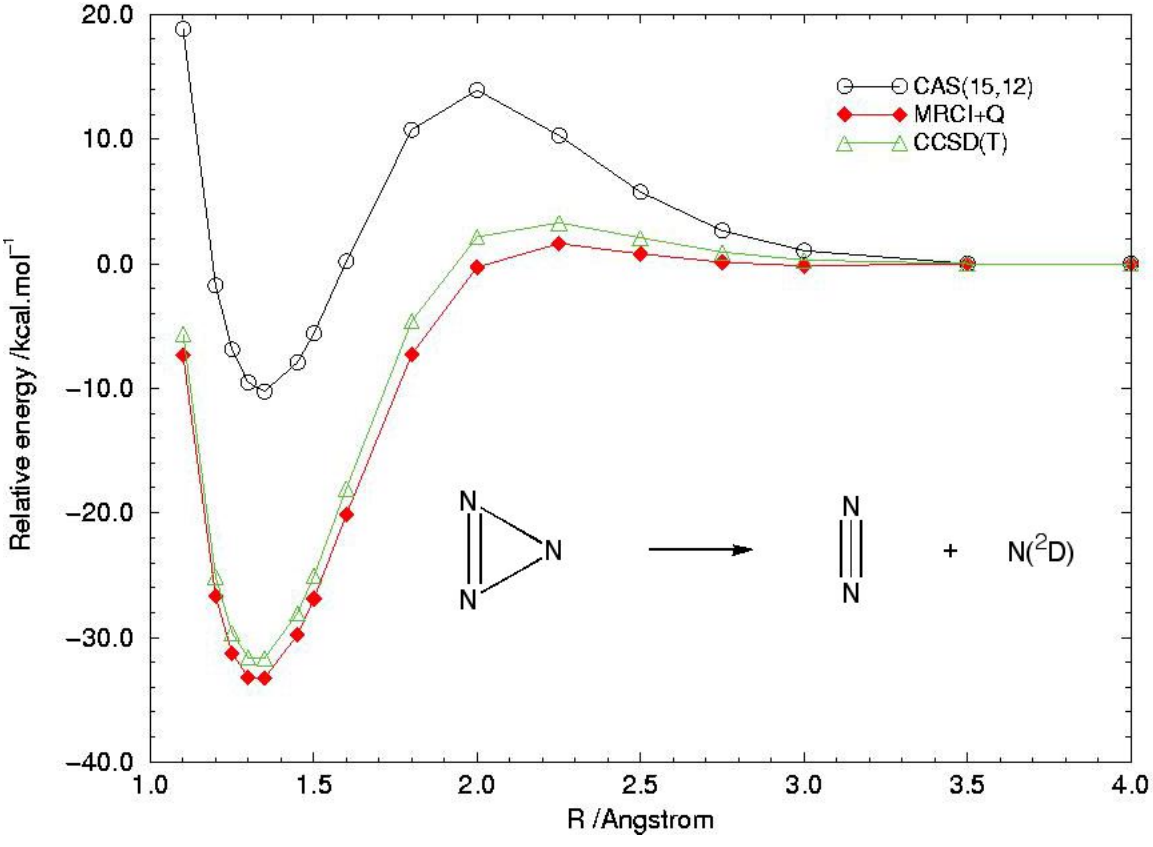

Fig. 37. The dissociation pathway of N_3(C_{2v}) calculated at various computational levels

The N_3 (C_{2v}) radical can be generated by the association of N(^{2}D) and ground state N_2. An analysis of the N_3 (C_{2v}) dissociation pathway at the MR-CISD(Q) level indicates that N_3 (C_{2v}) can be formed from these reactants with an activation energy of less than 1.5 kcal/mol. The dissociation energy of N_3 (C_{2v}) is close to 23 kcal/mol, which makes it sufficiently stable to be used as a precursor in N_4 (T_d) synthesis. The isomerization barrier for formation of the linear N_3 radical is also relatively high, 32 kcal/mol. However, it should be noted that also linear N_3 can be formed from N(^{2}D) and N_2 in a process with near zero barrier. In addition, our calculations indicate that reactive cross section for this process is larger than for the formation of N_3 (C_{2v}). Thus, it can be expected that N_3 (C_{2v}) will only be formed in relatively low concentrations.

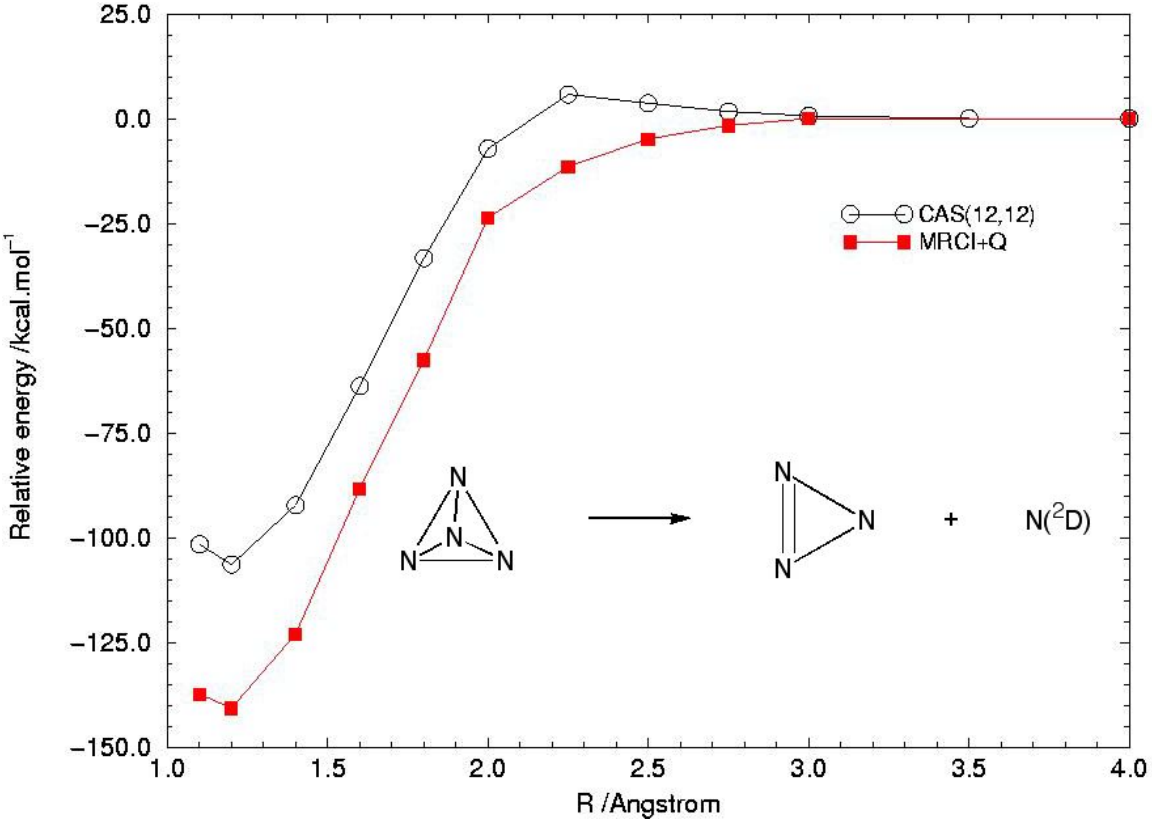

Fig. 38. Reaction pathway for the dissociation of N_4 (T_d) to N_3 (C_{2v}) and N(^{2}D) computed at the CAS(12,12)/VTZ and MRCI(Q)/VTZ levels of theory.

In the next step we investigated the reaction of N_3 (C_{2v}) with N(^{2}D) to form N_4 (T_d). A scan of the potential energy surface at the CAS(12,12) level indicates that a perpendicular approach of N(^{2}D) towards the N_3 (C_{2v}) molecular plane is most favorable for reaction. This can also be rationalized from an analysis of the occupied orbitals in the two species. The N_4 (T_d) dissociation pathway calculated at the MR-CISD(Q) level indicates that N_4 (T_d) can be formed from N_3 (C_{2v}) and N(^{2}D) in a barrierless reaction, as is expected for a radical recombination process. However, the scan of the potential energy surface shows that the reaction channel is rather narrow and that N_2 molecules may be formed in a competing process.

The possible existence of other stable N_4 isomers than N_4 (T_d) is of particular interest. We have recently reinvestigated the rectangular N_4 (D_{2h}) molecule using high level *ab initio* methods [12]. Our study indicates that this isomer is of similar energy as N_4 (T_d), but much less stable. A C_{2v} transition state towards dissociation (N_4 (D_{2h}) $\rightarrow$ 2 N_2) was located and characterized at the CAS(12,12)/VTZ level of theory. The effective dissociation barrier was estimated to 6.5 kcal/mol from MR-AQCC/VTZ calculations. This shows that N_4 (D_{2h}) is considerably more stable than was indicated in an earlier study, and that it may be possible to synthesize and isolate at low temperatures.

In order to produce reference data for optical detection we calculated vertical excitation energies and oscillator strengths for the lowest 20 singlet states of N_4 (D_{2h}) using the EOM-CCSD method. The lowest excited state (1^1B_{3u}), which also is the first optically accessible state, lies about 1.6 eV above the ground state. This excited state was optimized and found to be bound at a wide variety of computational levels, e.g. CASSCF, TD-B3LYP and EOM-CCSD. Its geometry is very similar to the ground state (Table 5), which results in large Frank-Condon factors for transitions between the two states. This fact, together with the very low excitation energy, indicates that the 1^1B_{3u} state will be useful for detection of N_4 (D_{2h}) by means of LIF spectroscopy.

Table 5. (EOM)-CCSD/AVDZ equilibrium structures (Å), harmonic frequencies (cm^{-1}), and excitation energies (eV) for the ground state and the first excited state of N_4 (D_{2h}).

State	Ground state (^1A_g)	First excited state ($^1B_{3u}$)
R_{12}	1.540	1.517
R_{13}	1.269	1.264
$\omega_1(a_u)$	489	606
$\omega_2(b_{2u})$	580	586
$\omega_3(a_g)$	957	980
$\omega_4(b_{3g})$	1048	580
$\omega_5(b_{1u})$	1421	1300
$\omega_6(a_g)$	1625	1650
ΔE_{vexc}	0.0	1.62
$\Delta E_{0\text{-}0}$	0.0	1.60

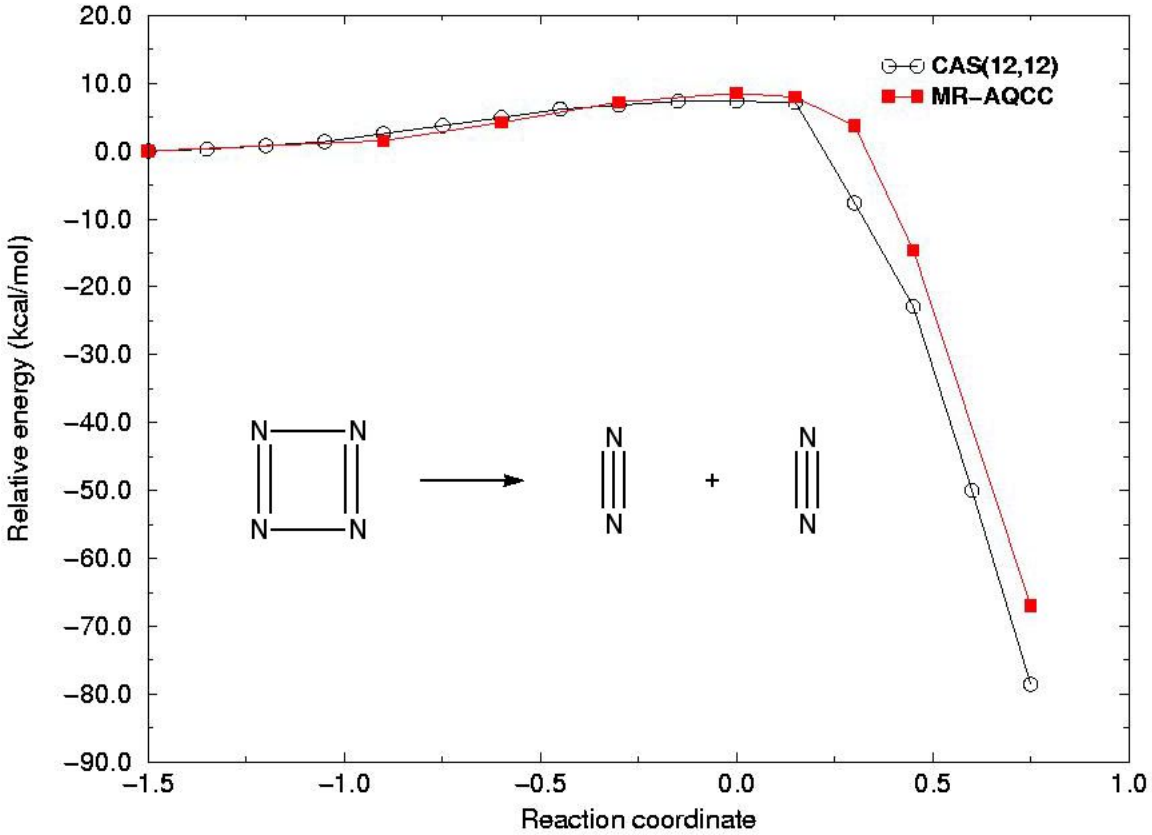

Fig. 39. The dissociation pathway of N_4 (D_{2h}) calculated at the CAS(12,12)/VTZ and MR-AQCC/VTZ levels.

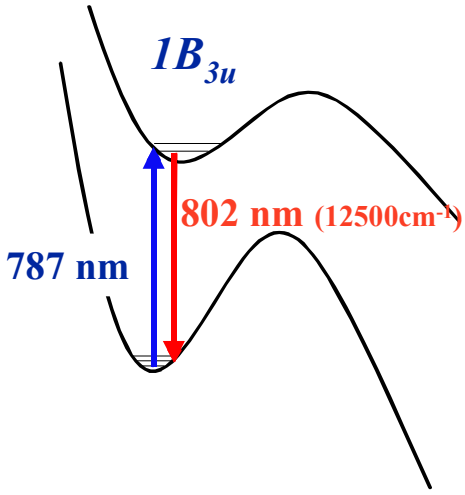

State	Excitation Energy[1] (eV)	Oscillator Strength[1]
$1B_{3u}$	1.57	0.0033
$2B_{3u}$	7.22	0.0008
$1B_{2u}$	8.58	0.0075
$1B_{1u}$	10.04	0.1883

1) EOM-CCSD / AVTZ

Fig. 40. Proposed LIF detection scheme for the rectangular $N_4(D_{2h})$ species.

Summary

Activities:

- A second cryostat has been set up for laser excitation experiments and preparations have been made for temperature-controlled matrix excitation experiments with Raman detection using the 514.5 nm line of an Ar^+ laser.
- Initial experiments have been made on excitation of liquid nitrogen with a 193 nm ArF laser.
- Ion bombardment, microwave-excitation and hollow-cathode excitation experiments of solid N_2 have been performed in two cryostats. Several synthesis experiments with long integration times have been carried out.
- Temperature-controlled matrix excitation experiments with Raman detection using the 514.5 nm line of an Ar^+ laser have been performed.
- A VUV detection system has been set up for studies of excitation processes in nitrogen-containing matrices.
- Initial experiments have been made on multiphoton excitation of liquid nitrogen in a capillary with a tunable dye laser.
- Decomposition experiments on heterocyclic high-nitrogen compounds have been carried out using detection with a time of flight mass spectrometer.
- SERS experiments have been performed on several previously characterized substances.
- Calibration experiments on $P_4(T_d)$ have been made at cryogenic temperatures.
- Extensive calculations have been performed on excited states of $N_4(T_d)$ and $N_4(D_{2h})$ in order to find high-sensitivity detection methods for N_4.

Progress:

- A number of unassigned features have been observed in ion bombarding, microwave-excitation and hollow-cathode excitation experiments on nitrogen-containing matrices.
- The Vegard-Kaplan bands of nitrogen have been produced at very high intensity levels in nitrogen and mixed argon-nitrogen matrices using ion gun excitation.
- SERS-active surfaces have been produced and successful SERS-experiments have been performed at room temperature.
- Excellent Raman spectra of $P_4(T_d)$ have been recorded at cryogenic temperatures.
- Possible decomposition routes have been established experimentally for several high-nitrogen compounds, using laser decomposition in combination with time of flight mass spectroscopy.
- The tetrahedral N_4^+ ion has been found to be stable in *ab initio* calculations.
- The rectangular $N_4(D_{2h})$ species has been found to be stable in *ab initio* calculations, and a LIF detection scheme has been proposed for its detection.

Reports:

- Four reports have been written (Refs. 1, 5, 10 and 17 in the reference list).
- Four articles have been published. (Refs 3, 4, 6 and 12 in the reference list).

Conference contribution:

- Poster presentation: *Synthesis Efforts and Detection of N_4 in Nitrogen Matrices* by Sara Wallin and Henric Östmark at the conference*: The Chemistry and Physics of Matrix Isolated Species*, July 7-13, 2001, Szklarska Poreba, Poland

References

1. H. Östmark, O. Launila, R. Tryman, S. Wallin, G. Petri, A. Pettersson, R. Claridge and N. Hore: *The N_4 project. Annual report for the year 2000.*
   Progress report FOA-R-00-01812-310-SE (2001)

2. H. Östmark, O. Launila, H. Bergman, J. Dahlberg, K. Ekvall and A. Pettersson: *The N_4 project. Laser synthesis experiments on N_2(liq).*
   Progress report FOA-R-99-01098-310-SE (1999)

3. M. Bittererova, T. Brinck and H. Östmark, *Theoretical Study of the Triplet N_4 Potential Energy Surface. J.Phys.Chem. A* **104**, 11999-12005 (2000)

4. H. Östmark, O. Launila, S. Wallin and R. Tryman, *On the Possibility of Detecting Tetraazatetrahedrane (N_4) in Liquid or Solid Nitrogen by FT-Raman Spectroscopy. J. Raman Spectrosc.* **32**, 195-199 (2001)

5. O. Launila, H. Östmark, R. Tryman, S. Wallin, G. Petri and A. Pettersson: *The N_4 project. Report for the first quarter of 2001.*
   Progress report FOI-R--0127--SE (2001)

6. M. Bittererová, T. Brinck and H. Östmark, *Theoretical study of the singlet electronically excited states of N_4. Chem. Phys. Lett.* **340**, 597-603 (2001)

7. J.P. Perchard, *Anharmonicity and hydrogen bonding II - A near infrared study of water trapped in nitrogen matrix. Chem. Phys.* **266**, 109-124 (2001)

8. J. R. Holden, Z. Du, and H. L. Ammon, *Journal of Computational Chemistry* **14,** 422-437 (1993).

9. Yu. A. Dmitriev and R. A. Zhitnikov, *Study of matrix isolation of nitrogen atoms in solid N_2, Low Temperature Physics* **24**, 284-290 (1998)

10. O. Launila, H. Östmark, R. Tryman, S. Wallin, G. Petri and A. Pettersson: *The N_4 project. Activity report for the first half of the year 2001.* Progress report FOI-R--0160--SE (2001)

11. H. Östmark, O. Launila, H. Bergman, J. Dahlberg, K. Ekvall and A. Pettersson: *The N_4 project. Laser synthesis experiments on N_2(liq).* Progress report FOA-R-99-01098-310-SE (1999)

12. M. Bittererová, H. Östmark and T. Brinck, *Ab initio study of the ground state and the first excited state of the rectangular (D_{2h}) N_4 molecule.* Chem. Phys. Lett., **347**, 220, (2001)

13. Japanese Patent Application, *Nitrogen polymer and its production*, Kokai Publications No Hei 11-43315, February 16, 1999

14. M. Bittererová and T. Brinck, private communication

15. E.V. Savchenko, O.N. Gigoraschenko, A.N. Ogurtsov, V.V. Rudenkov, M. Lorenz, M. Frankowski, A.M. Smith-Gicklhorn and V.E. Bondybey *Journal of Luminescence*, In press (2002)

16. E. Roth, G.A. Hope, D.P. Schweinsberg, W. Kiefer and P.M. Fredericks *Applied Spectroscopy* **47**, 1794-1799 (1993)

17. H. Östmark, M. Bittererová, H. Östmark, T. Brinck, N. Hore, R. Claridge, R. Tryman, S. Wallin, A. Pettersson and O. Launila: *The N_4 project. Activity report for the third quarter of 2001.* Progress report FOI-R--0223--SE (2001)